
Efficient Sensor Placement from Regression with Sparse Gaussian Processes in Continuous and Discrete Spaces

Kalvik Jakkala and Srinivas Akella*

Abstract We present a novel approach based on sparse Gaussian processes (SGPs) to address the sensor placement problem for monitoring spatially (or spatiotemporally) correlated phenomena such as temperature and precipitation. Existing Gaussian process (GP) based sensor placement approaches use GPs with known kernel function parameters to model a phenomenon and subsequently optimize the sensor locations in a discretized representation of the environment. In our approach, we fit an SGP with known kernel function parameters to randomly sampled unlabeled locations in the environment and show that the learned inducing points of the SGP inherently solve the sensor placement problem in continuous spaces. Using SGPs avoids discretizing the environment and reduces the computation cost from cubic to linear complexity. When restricted to a candidate set of sensor placement locations, we can use greedy sequential selection algorithms on the SGP’s optimization bound to find good solutions. We also present an approach to efficiently map our continuous space solutions to discrete solution spaces using the assignment problem, which gives us discrete sensor placements optimized in unison. Moreover, we generalize our approach to model sensors with non-point field-of-view and integrated observations by leveraging the inherent properties of GPs and SGPs. Our experimental results on three real-world datasets show that our approaches generate solution placements that result in reconstruction quality that is consistently on par or better than the prior state-of-the-art approach while being significantly faster. Our computationally efficient approaches will enable both large-scale sensor placement, and fast sensor placement for informative path planning problems.

1 Introduction

Meteorology and climate change are concerned with monitoring correlated phenomena of an environment such as temperature, ozone concentration, soil chemistry, ocean salinity, and fugitive gas density (Krause et al. [2008], Whitman et al. [2021], Suryan and Tokekar [2020], Ma et al. [2017], Jakkala and Akella [2022]). However, it is often too expensive and, in some cases, even infeasible to monitor the entire environment with a dense sensor network. We therefore aim to determine strategic locations for a small set of sensors so that the data from these sensors gives us the most accurate estimate of the phenomenon over the entire environment. We address this *sensor placement problem* for spatially (or spatiotemporally) correlated environment monitoring.

The sensor placement problem in correlated environments is a fundamental problem with diverse and important applications. For example, informative path planning (IPP) is a crucial problem in robotics that involves identifying informative sensing locations for a robot while considering distance constraints (Ma et al. [2017]). Similar sensor placement problems arise in autonomous robot inspection and monitoring of 3D surfaces (Zhu et al. [2021]), for example when a robot must monitor stress fractures on a 3D aircraft body. Tomography is another important field in which one has to recover an underlying data field from integrated sensor data. The problem is often studied in computerized tomography (CT) and requires informative sensor placement (Longi et al. [2020]). Fugitive gas density estimation in oil fields using tunable diode laser absorption spectroscopy

*The authors are with the Computer Science Department, University of North Carolina at Charlotte, Charlotte, NC, USA. Email: {kjakkala, sakella}@uncc.edu. This work was funded in part by the UNC Charlotte Office of Research and Economic Development and by NSF under Award Number IIP-1919233.

sensors that report the integrated gas concentration is a closely related problem that requires sensor placement (Arain et al. [2016]). Additionally, phenomena like magnetic fields in nuclear reactors are subject to linear constraints (Jidling et al. [2017]) and can benefit from sensor placements that leverage the system dynamics.

Solving the sensor placement problem requires finding a small set of locations to place sensors such that they cover the whole environment. Such problems have been addressed using well-established computational geometry approaches (de Berg et al. [2008]), but they are only designed to cover the environment without leveraging the correlations in the environment.

An effective approach to model spatially correlated data is to use Gaussian processes (GPs) (Krause et al. [2008], Shewry and Wynn [1987], Wu and Zidek [1992], Husain and Caselton [1980]). We can then leverage the GPs to estimate information metrics such as mutual information (MI). Such metrics can be used to quantify the amount of new information that can be obtained from each candidate sensor location. However, computing MI using GPs is very expensive as it requires the inversion of large covariance matrices whose size increases with the environment’s discretization resolution. Having faster sensor placement approaches would enable addressing the abovementioned applications which require a large number of sensor placements or a fine sensor placement precision that is infeasible with discrete approaches.

We show that every sparse Gaussian process (SGP) trained for regression tasks also solves a sensor placement problem very efficiently. SGPs (Quinero-Candela et al. [2007], Bui et al. [2017]) are a computationally efficient variant of GPs with a reduced computation cost that is linear in the number of training samples. Most of the SGP literature has focused on using SGPs only as a faster variant of GPs. One might consider replacing the full GP with an SGP in GP-based approaches for faster sensor placement. But given how GPs are used in sensor placement approaches, we would have to train a new SGP for every evaluation of information metrics such as MI. And since such sensor placement approaches involve repeated evaluations of MI, the computational cost of training the SGPs will be higher than the original full GP-based approach. As such, a naive replacement of GPs with SGPs will be inefficient.

Instead, we reason that SGPs can be more than just an information metric measurement tool in GP-based sensor placement approaches. Indeed, we show that SGPs inherently solve our sensor placement problem when trained on randomly sampled unlabeled locations. In contrast to earlier GP-based approaches that can handle only discrete sensor placement, our approach can be used to efficiently solve the sensor placement problem for both continuous and discrete sensor placements. Our contributions are as follows:

1. This article presents an efficient gradient-based approach for sensor placement in continuous environments by uncovering the connection between sparse Gaussian processes and a rich class of sensor placement problems.
2. We present an efficient assignment problem-based method to map our continuous space solutions to discrete solution spaces. So our approach can even be used for sensor placement in discrete environments.
3. We generalize our approach to leverage the properties of GPs and SGPs to model challenging sensor models such as sensors with non-point field-of-view (FoV) and integrated observations.

2 Problem Statement

Consider a spatially (or spatiotemporally) correlated stochastic process Ψ over an environment $\mathcal{V} \subseteq \mathbb{R}^d$ modeling a phenomenon such as temperature. A set \mathcal{A} of s sensor locations $\{\mathbf{x}_i \in \mathcal{V}, i = 1, \dots, s\}$ must be selected so that the phenomenon data $y_i \in \mathbb{R}$ collected at these locations gives us the most accurate estimate of the phenomenon at every location in the environment. We consider estimates with the lowest root-mean-square error (RMSE) as the most accurate. We initially model point sensors with Gaussian noise and later also consider non-point sensors with an arbitrary field of view (FoV) and Gaussian noise. We consider both continuous sensor placements $\mathcal{A} \subseteq \mathcal{V}$ and discrete sensor placements $\mathcal{A} \subseteq \mathcal{S} \subseteq \mathcal{V}$, where \mathcal{S} is a given discrete set of candidate sensor locations. We are given a small dataset from the environment to learn the spatial correlations or have the domain knowledge to describe how the space is correlated. An ideal solution to this *sensor placement problem* ensures accurate estimation of the phenomenon by leveraging its correlations to optimize the placements.

3 Background: GPs and SGPs

Gaussian processes (GPs, Rasmussen and Williams [2005]) are a non-parametric Bayesian approach that we can use for regression, classification, and generative problems. Suppose we are given a regression task's training set $\mathcal{D} = \{(\mathbf{x}_i, y_i), i = 1, \dots, n\}$ with n data samples consisting of inputs $\mathbf{x}_i \in \mathbb{R}^d$ and noisy labels $y_i \in \mathbb{R}$, such that, $y_i = f(\mathbf{x}_i) + \epsilon_i$, where $\epsilon_i \sim \mathcal{N}(0, \sigma_{\text{noise}}^2)$. Here σ_{noise}^2 is the variance of the independent additive Gaussian noise in the observed labels y_i , and the latent function $f(\mathbf{x})$ models the noise-free function of interest that characterizes the regression dataset.

GPs model such datasets by assuming a GP prior over the space of functions that we could use to model the dataset, i.e., they assume the prior distribution over the function of interest $p(\mathbf{f}|\mathbf{X}) = \mathcal{N}(0, \mathbf{K})$, where $\mathbf{f} = [f_1, f_2, \dots, f_n]^\top$ is a vector of latent function values, $f_i = f(\mathbf{x}_i)$. $\mathbf{X} = [\mathbf{x}_1, \mathbf{x}_2, \dots, \mathbf{x}_n]^\top$ is a vector (or matrix) of inputs, and $\mathbf{K} \in \mathbb{R}^{n \times n}$ is a covariance matrix, whose entries \mathbf{K}_{ij} are given by the kernel function $k(\mathbf{x}_i, \mathbf{x}_j)$.

GPs use the kernel function to index the inputs \mathbf{X} so that points closer to each other (i.e., with high covariance value from the kernel function) have similar labels and vice versa. The kernel function parameters are tuned using Type II maximum likelihood (Bishop [2006]) so that the GP accurately predicts the training dataset labels. We can compute the posterior of the GP with the mean and covariance functions:

$$\begin{aligned} m_{\mathbf{y}}(\mathbf{x}) &= \mathbf{K}_{x\mathbf{n}}(\mathbf{K}_{\mathbf{n}\mathbf{n}} + \sigma_{\text{noise}}^2 I)^{-1} \mathbf{y}, \\ k_{\mathbf{y}}(\mathbf{x}, \mathbf{x}') &= k(\mathbf{x}, \mathbf{x}') - \mathbf{K}_{x\mathbf{n}}(\mathbf{K}_{\mathbf{n}\mathbf{n}} + \sigma_{\text{noise}}^2 I)^{-1} \mathbf{K}_{\mathbf{n}x'}, \end{aligned} \quad (1)$$

where \mathbf{y} is a vector of all the outputs, and the covariance matrix subscripts indicate the variables used to compute it, i.e., $\mathbf{K}_{\mathbf{n}\mathbf{n}}$ is the covariance on the training inputs \mathbf{X} , and $\mathbf{K}_{x\mathbf{n}}$ is the covariance between the test input \mathbf{x} and the training inputs \mathbf{X} . This approach requires an inversion of a matrix of size $n \times n$, which is a $\mathcal{O}(n^3)$ operation, where n is the number of training set samples. Thus this method can handle at most a few thousand training samples.

Sparse Gaussian processes (SGPs) (Snelson and Ghahramani [2006], Bui et al. [2017], Titsias [2009], Hoang et al. [2015]) address the computational cost issues of Gaussian processes. SGPs do this by approximating the full GP using another Gaussian process supported with m data points called *inducing points*, where $m \ll n$. Since the SGP support set (i.e., the data samples used to estimate the training set labels) is smaller than the full GP's support set (the whole training dataset), SGPs reduce the matrix inversion cost to $\mathcal{O}(m^3)$.

There are multiple SGP approaches; one particularly interesting approach is the sparse variational GP (SVGP, Titsias [2009]), which is the most well-known approach in the Bayesian community and has had a significant impact on the Gaussian process literature given its theoretical properties (Burt et al. [2019], Bauer et al. [2016]).

To approximate the full GP, the SVGP approach uses a variational distribution q parametrized with m inducing points. The approach treats the inducing points as variational parameters instead of model parameters, i.e., the inducing points parametrize a *distribution* over the latent space of the SGP instead of directly parametrizing the latent space. Thus the inducing points are protected from overfitting. The SVGP approach's mean predictions and covariances for new data samples are computed using the following equations:

$$\begin{aligned} m_{\mathbf{y}}^q(\mathbf{x}) &= \mathbf{K}_{x\mathbf{m}} \mathbf{K}_{\mathbf{m}\mathbf{m}}^{-1} \boldsymbol{\mu}, \\ k_{\mathbf{y}}^q(\mathbf{x}, \mathbf{x}') &= k(\mathbf{x}, \mathbf{x}') - \mathbf{K}_{x\mathbf{m}} \mathbf{K}_{\mathbf{m}\mathbf{m}}^{-1} \mathbf{K}_{\mathbf{m}x'} + \mathbf{K}_{x\mathbf{m}} \mathbf{K}_{\mathbf{m}\mathbf{m}}^{-1} \mathbf{A} \mathbf{K}_{\mathbf{m}\mathbf{m}}^{-1} \mathbf{K}_{\mathbf{m}x'}, \end{aligned} \quad (2)$$

where the covariance term subscripts indicate the input variables used to compute the covariance; m corresponds to the inducing points \mathbf{X}_m and x corresponds to any other data point \mathbf{x} . $\boldsymbol{\mu}$ and \mathbf{A} are the mean and covariance of the optimal variational distribution q^* . The approach maximizes the following evidence lower bound (ELBO) \mathcal{F} to optimize the parameters of the variational distribution:

$$\mathcal{F} = \underbrace{\frac{n}{2} \log(2\pi)}_{\text{constant}} + \underbrace{\frac{1}{2} \mathbf{y}^\top (\mathbf{Q}_{\mathbf{n}\mathbf{n}} + \sigma_{\text{noise}}^2 I)^{-1} \mathbf{y}}_{\text{data fit}} + \underbrace{\frac{1}{2} \log |\mathbf{Q}_{\mathbf{n}\mathbf{n}} + \sigma_{\text{noise}}^2 I|}_{\text{complexity term}} - \underbrace{\frac{1}{2\sigma_{\text{noise}}^2} \text{Tr}(\mathbf{K}_{\mathbf{n}\mathbf{n}} - \mathbf{Q}_{\mathbf{n}\mathbf{n}})}_{\text{trace term}}, \quad (3)$$

where $\mathbf{Q}_{nn} = \mathbf{K}_{nm}\mathbf{K}_{mm}^{-1}\mathbf{K}_{mn}$ and \mathbf{K}_{mm} is the covariance matrix of the inducing points \mathbf{X}_m . The lower bound \mathcal{F} has three key terms. The data fit term ensures that the training set labels are accurately predicted. The complexity and trace terms are independent of the labels. The complexity term ensures that the inducing points are spread apart to ensure good coverage of the whole training set, and the trace term represents the sum of the variance of the conditional $p(\mathbf{f}|\mathbf{f}_m)$. Here \mathbf{f}_m are the latent variables corresponding to the inducing point inputs \mathbf{X}_m . When the trace term becomes zero, the m solution inducing points become a sufficient statistic for the n training samples, i.e., an SGP with only the m solution inducing points can make the same predictions as a GP with all the n samples in its training set. Please refer to Bauer et al. [Bauer et al. 2016] for an in-depth analysis of the SVGP’s lower bound. We present additional related work in the appendix because of space constraints.

4 Methods

Our sensor placement approach leverages the inherent characteristics of SGPs (Rasmussen and Williams [2005], Snelson and Ghahramani [2006], Titsias [2009], Bui et al. [2017]) to efficiently and accurately place sensors in an environment. Given a training dataset with n samples, SGPs select a small set of m inducing points, where $m \ll n$. The inducing points are selected to approximate the training dataset accurately. We can then use only the inducing points to predict the labels of the test dataset. Since SGPs use only the inducing points instead of the whole training data to predict the test set labels, the approach is computationally cheaper ($\mathcal{O}(nm^2)$) than using a full GP ($\mathcal{O}(n^3)$). We solve the sensor placement problem by fitting an SGP to locations from the environment and interpreting the resulting inducing points as the sensor locations. In addition, unlike conventional SGPs that use labeled training data, we instead use an unlabeled approach to train them; this allows us to find sensor placements even in unobserved environments.

We use randomly sampled unlabeled locations in the environment as the inputs of the training set. Since SGPs are usually trained on labeled datasets, we set all the training set labels and the SGP mean function to zero; this allows us to train the SGP on our unlabeled dataset. Similar to earlier GP-based sensor placement approaches, our approach assumes that we know the kernel parameters, either learned from a small set of historical data that could even be from a subregion of the environment, or from domain knowledge. Thus our SGP accounts for the correlations of the data field encoded in the kernel function while optimizing the inducing points. Also, since we only need to optimize the inducing point locations, we can do it independent of the training set labels, which in our case are all set to zero. We can impose a cardinality constraint over the solution sensor placements by specifying the number of inducing points used in the SGP.

Unlike earlier sensor placement approaches (Krause et al. [2008], Wu and Zidek [1992]), our solution allows sensors to be placed anywhere in a continuous environment. In addition, our solution enables leveraging the vast SGP literature to address multiple variants of the sensor placement problem. For example, we can use sparse variational GPs (SVGPs, Titsias [2009]) with our approach to address the problem in spatially correlated environments. We can use stochastic gradient optimizable SGPs (Wilkinson et al. [2021]) with our approach to address significantly large sensor placement problems, i.e., environments that require a large number of sensor placements. Similarly, we can use spatiotemporal-SVGPs (Hamelijnck et al. [2021]) with our approach to efficiently optimize sensor placements for spatiotemporally correlated environments.

Also, when using the SVGP approach (Titsias [2009]), which has good convergence properties (Matthews et al. [2016], Bauer et al. [2016], Burt et al. [2019]), fitting it on our unlabeled dataset corresponds to optimizing the complexity and trace terms of the SVGP’s lower bound \mathcal{F} (Equation 3). The complexity term ensures good coverage, i.e., well-separated sensor placements, and the trace term ensures that the uncertainty about the entire environment is minimized given the data from the solution placements. In addition, both terms leverage the environment’s covariance structure captured by the kernel function to better use the available sensors.

In the remainder of this section, we detail our approach for continuous space sensor placement using gradient descent, discrete space placement using a greedy algorithm, and discrete space placement using the continuous space placements along with a mapping technique. We then present an approach to generalize our sensor placement methods for sensors with non-point FoV and integrated observations, and detail how we can handle obstacles in the environment. Finally, we juxtapose our approach with a mutual information (MI) based sensor placement approach (Krause et al. [2008]).

4.1 Continuous-SGP: Continuous Solutions

We solve the continuous space sensor placement problem using randomly sampled unlabeled locations in the environment as the SGP’s training set inputs. We set the training set labels to zero and initialize an SVGP (Titsias [2009]) with a pretrained kernel function. All the inducing points of the SGP are simultaneously optimized using gradient descent and are used as the solution sensor locations. We provide the pseudocode for this method in Algorithm 1.

4.2 Greedy-SGP: Greedy Discrete Solutions

Now consider the case when we want to limit the solution of the sensor placement problem to a discrete set of candidate locations, either a subset of the training points or any other arbitrary set of points. In this case, we can use the inducing points selection approach outlined in Titsias [2009] to handle non-differentiable data domains. The approach entails sequentially selecting the inducing points \mathbf{X}_m from the candidate set \mathcal{S} using a greedy approach (Equation 4). It considers the increment in the SVGP’s optimization bound \mathcal{F} as the maximization criteria. In each iteration, we select the point \mathbf{x} that results in the largest increment in the SVGP’s bound \mathcal{F} upon being added to the current inducing points set \mathbf{X}_m ²:

$$\mathbf{X}_m \leftarrow \mathbf{X}_m \cup \left\{ \arg \max_{\mathbf{x} \in \mathcal{S} \setminus \mathbf{X}_m} \mathcal{F}(\mathbf{X}_m \cup \{\mathbf{x}\}) - \mathcal{F}(\mathbf{X}_m) \right\}. \quad (4)$$

Here \mathbf{X}_m is the set of inducing points/sensing locations, and $\mathcal{S} \setminus \mathbf{X}_m$ is the set of remaining candidate locations after excluding the current inducing points set \mathbf{X}_m .

4.3 Discrete-SGP: Gradient-based Discrete Solutions

The problem with any greedy selection algorithm is its inherently sequential selection procedure. A better solution may be possible if the initially selected inducing points are re-selected at the end of the greedy approach, or if the inducing points are all selected together while accounting for their combined effect instead of only incrementally considering the effect of the ones that were selected in the sequential approach.

Our approach to this problem is to simultaneously optimize all the inducing points in the continuous input space using gradient descent (as in Section 4.1) and map the solution to the discrete candidate solution space \mathcal{S} . We can map the continuous space solutions to discrete sets by treating the mapping problem as an assignment problem (Burkard et al. [2012]), i.e., as a weighted bipartite matching problem. The assignment problem requires one to find the minimal cost matching of a set of items to another set of items given their pairwise costs. We compute the pairwise Euclidean distances between the continuous space inducing points and the discrete space candidate set locations \mathcal{S} . The distances are then used as the costs in an assignment problem. One could even use covariances that are appropriately transformed, instead of distances, in the mapping operation to account for the correlations in the environment.

The solution of the assignment problem gives us points in the discrete candidate set closest to the continuous space solution set². Such a solution could be superior to the greedy solution since the points in the continuous space solution set are simultaneously optimized using gradient descent instead of being sequentially selected. Although the gradient-based solution could get stuck in a local optimum, in our experiments, we found that the gradient-based discrete solutions are on par or better than the greedy solutions while being substantially faster to optimize.

4.4 Linear and Non-linear transformations in SGPs

Consider the problem of sensor placement for sparse view CT (Longi et al. [2020]). A third-generation fan beam CT scanner (Zeng [2017]) projects X-ray beams that fan out at a fixed angle (Figure 1).

² We provide the pseudocode for our algorithms in the Appendix.

Algorithm 1: Continuous-SGP. k_θ is the kernel with learned parameters, Φ is a random distribution defined over the domain of the environment \mathcal{V} , and γ is the SGP learning rate.

Input: $k_\theta, \mathcal{V}, \Phi, s, n, \gamma$

Output: Sensor placements $\mathcal{A} \subset \mathcal{V}, |\mathcal{A}| = s$

$\mathbf{X} \sim \Phi(\mathcal{V})$ // Draw n unlabeled locations

$\mathbf{X}_m = \text{RandomSubset}(\mathbf{X}, s)$ // Initialize \mathbf{X}_m

// Initialize SVGP with 0 label dataset

$\varphi = \text{SGP}(\text{mean} = 0, k_\theta; \mathbf{X}, \mathbf{y} = \mathbf{0}, \mathbf{X}_m)$

Loop until convergence: $\mathbf{X}_m \leftarrow$

$\mathbf{X}_m + \gamma \nabla \mathcal{F}_\varphi(\mathbf{X}_m)$

return \mathbf{X}_m

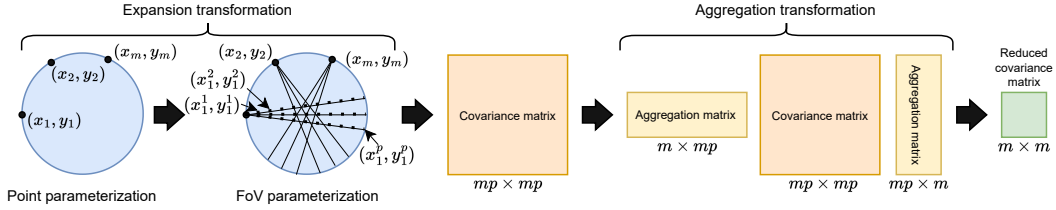


Figure 1: An illustration of the sensor placement approach for sparse view CT scanning with fan beam projections. The expansion transformation maps each of the m inducing points in the point parametrization to p points in the FoV parametrization to approximate each sensor’s FoV.

On the opposite side of the projector, a sensor array captures data integrated along each beam and encoded by the received X-ray intensity. The projector and sensor array pair rotate around a circular area of interest, and the collected data is then used to reconstruct the underlying spatially resolved data. Being able to efficiently compute informative sensor placements is especially useful when the region of interest is a sub-region of the observation space (e.g., if we only need to scan a specific organ), as we will be able to optimize the sensor placements in real-time, thereby reducing the amount of harmful X-ray exposure to the patients while also retaining the reconstruction quality.

A key advantage of our sensor placement approach is that we can leverage all the properties of GPs and SGPs. We detail two such properties and how they are used to address sensor placement for sensors with non-point FoV and integrated observations.

The first property is that the inducing points of SGPs can be transformed with any non-linear function and still be optimized using backpropagation and gradient descent. We can use such transformations to approximate the FoV of sensor with non-point FoV. We do this by parameterizing each inducing point of the SGP as a point on the edge of the circular observation space. To account for the information from each sensor’s whole FoV (X-ray beams within the fan angle), we apply a transformation—the expansion transformation T_{exp} —to map each inducing point to a set of p points that approximate the region within the corresponding sensor’s FoV as follows: $\mathbf{X}_{mp} = T_{\text{exp}}(\mathbf{X}_m)$. The expansion transformation is applied to the inducing points $\mathbf{X}_m \in \mathbb{R}^{m \times \bar{d}}$ to get the FoV parametrized inducing points $\mathbf{X}_{mp} \in \mathbb{R}^{mp \times d}$ before computing any covariance matrix involving the inducing points. Thus, we can still calculate the gradients for the inducing points with the point parametrization. Here \bar{d} is the dimension of the inducing points with point parametrization, and d is the dimension of the sensor placement environment \mathcal{V} .

The second property we utilize is that GPs are closed under linear transformations (Rasmussen and Williams [2005]). We can leverage the property to model sensors with integrated observations (Longi et al. [2020]), i.e., where the labels are modeled as $y_i = \|\mathbf{w}_i\| \int_0^1 f(\mathbf{w}_i t + \mathbf{z}_i) dt + \epsilon_i$, with \mathbf{z}_i as the start point of a line along which the data is integrated, and \mathbf{w}_i as the direction and length of the line. We do this with the aggregation transformation T_{agg} , which aggregates (with an averaging operation) the covariances corresponding to the p points that approximate each sensor’s FoV and reduces the size of the covariance matrix back to $m \times m$.

We first use the expansion transformation (T_{exp}) on the m inducing points to map them from point parametrization to a larger set of mp points. Then we use the aggregation transformation T_{agg} on covariance matrices built using the mp points, i.e., a $mp \times mp$ covariance matrix is reduced to an $m \times m$ covariance matrix (term in parentheses in Equation 5). We use the covariances to compute the SVGP’s lower bound (Equation 3) by evaluating \mathbf{Q}_{nn} :

$$\mathbf{Q}_{nn} = \mathbf{K}_{n \times mp} T_{\text{agg}} (T_{\text{agg}}^\top \mathbf{K}_{mp \times mp} T_{\text{agg}})^{-1} T_{\text{agg}}^\top \mathbf{K}_{mp \times n}. \quad (5)$$

Here $\mathbf{K}_{n \times mp}$ is the covariance between the n training set inputs and the mp inducing points. The approach is illustrated in Figure 1, and further details of how to define the transformations are presented in the appendix. The aggregation transformation reduces the covariance matrices before inversion. Therefore, the inversion operation cost is reduced to $\mathcal{O}(m^3)$ from $\mathcal{O}(m^3 p^3)$. Thus we reap the benefits of the compact point parametrization from the expansion transformation and the reduced computation cost from the aggregation transformation. We found that the aggregation transformation also stabilized the gradients while training the inducing points.

4.5 Obstacle Avoidance

We handle obstacles in the environment by building an appropriate training dataset for the SGP. We remove the random unlabeled samples in the SGP training set at locations in the interior of obstacles. Therefore the resulting training set has samples only in obstacle-free regions. Training an SGP on such data would result in inducing points that avoid the obstacles since placing the inducing points at locations with obstacles would not increase the likelihood of the training data used to optimize the SGP. Our obstacle avoidance approach is best suited for relatively large obstacles and ensures that the FoVs of most of the solution sensor placements do not overlap with obstacles.

5 Comparison with the Mutual Information Approach

Our SGP-based greedy approach (Equation. 4) has a few interesting similarities to the mutual information (MI) based sensor placement approach of Krause et al. [2008]. The MI approach uses a full GP to evaluate MI between the sensing locations and the rest of the environment to be monitored. The MI based criteria shown below was used to greedily select sensing locations:

$$MI(\mathbf{X}_m \cup \{\mathbf{x}\}) - MI(\mathbf{X}_m) = H(\mathbf{x}|\mathbf{X}_m) - H(\mathbf{x}|\mathcal{S}\setminus\mathbf{X}_m), \quad (6)$$

where \mathbf{X}_m is the set of selected sensing locations, and $\mathcal{S}\setminus\mathbf{X}_m$ is the set of all candidate locations in the environment excluding the current sensor locations \mathbf{X}_m . Krause et al. [2008] used a Gaussian process (GP) with known kernel parameters to evaluate the entropy terms. The SVGP’s optimization bound based selection criterion (Equation. 4) to obtain discrete solutions using the greedy algorithm is equivalent to maximizing the following $\Delta\mathcal{F}$ (derived in the Appendix):

$$\Delta\mathcal{F} = \text{KL}(\phi(f_i|\mathbf{f}_m)||p(f_i|\mathbf{y})) - \text{KL}(p(f_i|\mathbf{f}_m)||p(f_i|\mathbf{y})). \quad (7)$$

The first KL term measures the divergence between the variational distribution ϕ over f_i (the latent variable corresponding to \mathbf{x}) given the latents of the inducing points set \mathbf{X}_m , and the exact conditional given the training set labels \mathbf{y} (the conditional uses the training set inputs \mathbf{X} as well). The second term acts as a normalization term that measures the divergence between the exact conditional over f_i given the latents of the inducing points and the same given the training set labels.

A key difference between our and the MI approach is that we use the efficient cross-entropy (in the KL terms) to account for the whole environment. In contrast, the MI approach uses the computationally expensive entropy term $H(\mathbf{x}|\mathcal{S}\setminus\mathbf{X}_m)$. Given their overall similarities, $\Delta\mathcal{F}$ behaves similar to MI while being faster to compute; we empirically validate this in the experiments section.

Also, consider the limiting case where the SGP has the same number of inducing points as the number of candidate locations, i.e., we sense every location in the candidate set. In such a case, the two distributions in the KL-divergence would become equivalent, and the value would become zero. This is consistent with what we want since there will be no benefit in placing more sensors if all the locations are already being sensed.

Even in the continuous solution space, the SVGP’s lower bound (Equation 3) is similar to the MI approach. The trace term of the lower bound attempts to reduce the uncertainty about the whole environment, similar to the MI approach. However, the SVGP approach has the added complexity term, which ensures that we do not place the sensors too close to each other, thereby improving our solution quality.

6 Experiments

We demonstrate our methods on three datasets—Intel lab temperature (Bodik et al. [2004]), precipitation (Bretherton et al. [1999]), and COVID-19 CT scans (Jun et al. [2020]). The datasets are representative of real-world sensor placement problems and have been previously used as benchmarks (Krause et al. [2008]). We used an RBF kernel (Rasmussen and Williams [2005]) in all our experiments. However, one can also use non-stationary kernels with our approach.

The Intel lab dataset contains indoor temperature data collected from 54 sensors deployed in the Intel Berkeley Research lab from February 28th to April 5th, 2004. We used data from the first day of the dataset to learn the kernel parameters. The precipitation dataset contains daily precipitation data

around Oregon, U.S.A, in 1994. We used the first 10% of the data to learn the kernel parameters. The COVID-19 CT scan dataset contains lung scans from 10 patients, with each containing 301 slices.

We evaluated our approach using the root-mean-square error (RMSE). For the Intel lab and precipitation datasets, we used a GP parametrized with the pre-trained kernel function and the labeled data used to train the kernel function to sample a 50×50 grid of data for testing; this represents a realization of the phenomenon being monitored and ensures that we consider only the spatial correlations in the data. To obtain our estimate of the data field from the sensor placements, we used the sampled data at only the sensor locations to predict the data field at the remaining grid locations using Gaussian conditioning. We repeated the sampling and data field estimation process 100 times and reported the average RMSE between the sampled data and our predictions. We also report the SGP KL bound and mutual information in the Appendix.

We benchmarked our approaches—Continuous-SGP, Greedy-SGP, and Discrete-SGP. Here, Continuous-SGP (Section 4.1) is the solution obtained by using the inducing points learned by optimizing an SGP using gradient descent. Greedy-SGP (Section 4.2) is the solution obtained by selecting an SGP’s inducing points using a greedy approach (Equation. 4). Finally, Discrete-SGP (Section 4.3) is the solution obtained by mapping the Continuous-SGP solution to the discrete candidate sensor placement locations by solving the assignment problem. We also evaluated the performance of the MI approach (Krause et al. [2008]) as a baseline for comparison.

We computed the solution sensor placements for 1 to 29 sensors (in increments of 2) in the Intel lab and precipitation datasets. Since the candidate set is much larger in the precipitation dataset, we also computed the solution for up to 100 sensor placements (in increments of 10). Figures 2a and 2b show the RMSE values plotted against the number of required sensor placements. In the Intel lab dataset, our approaches—Continuous-SGP, Greedy-SGP, and Discrete-SGP—perform on par with the mutual information approach. Furthermore, given the larger candidate placement set in the precipitation dataset, our approaches are consistently better than the MI approach.

The Continuous-SGP and Discrete-SGP approaches simultaneously optimize all the placements and consider the combined effect of all the sensors’ estimate of the environment together. But since we use gradient descent, our two gradient-based approaches can get stuck in local minima. Nonetheless, our experiments show that our approaches are consistently on par with the greedy approach.

Figures 3a and 3b show the algorithm runtimes plotted against the number of required sensor placements. Our approaches are substantially faster than the MI approach. Indeed, in the Intel lab dataset, our Continuous-SGP approach is up to 3.7 times faster than the MI approach and up to 16 times faster in the precipitation dataset. Our SGP-based approaches need to invert only an $m \times m$ covariance matrix ($m \ll |\mathcal{S}|$, where $|\mathcal{S}|$ is the number of candidate locations). In contrast, the MI approach needs to invert up to an $|\mathcal{S}| \times |\mathcal{S}|$ covariance matrix to place each sensor, which takes

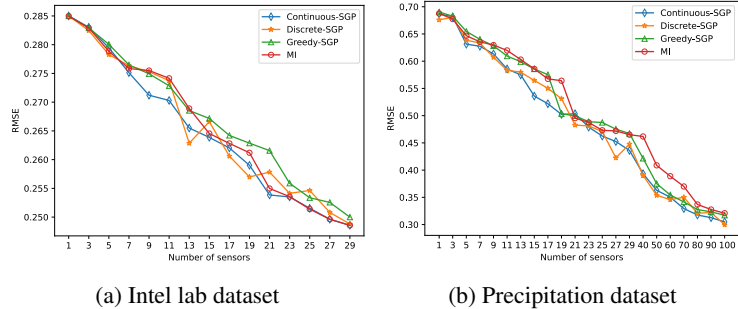


Figure 2: RMSE vs number of sensors for the Intel and precipitation datasets (lower is better).

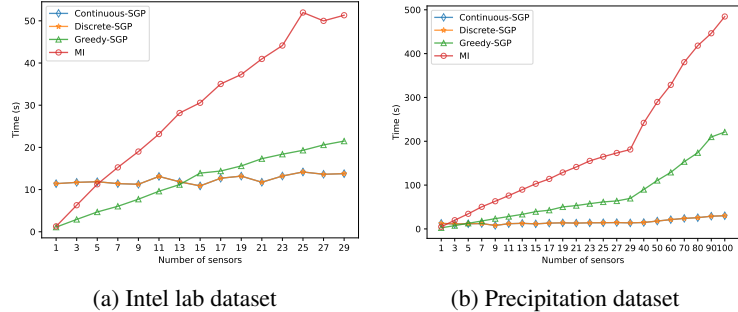


Figure 3: Runtime vs number of sensors for the Intel and precipitation datasets (lower is better).

$\mathcal{O}(|\mathcal{S}|^3)$ time. As such, the computation cost difference is further exacerbated in the precipitation dataset, which has over twice as many candidate sensor locations as the Intel lab dataset.

Solving the assignment problem in our Discrete-SGP approach to map the continuous gradient-based solution to the discrete candidate set incurs a one-time $\mathcal{O}(m^3)$ computation time that is negligible. Therefore our gradient-based approaches—Continuous-SGP and Discrete-SGP—converge at almost the same rate. Yet the Discrete-SGP retains the solution quality of the continuous solution.

Note that one can even use non-stationary kernel functions (Rasmussen and Williams [2005]) to capture intricate correlation patterns if the environment is known to be non-stationary. Also, the labeled locations in the Intel lab dataset used to train our kernel function did not align with our candidate locations. We chose this setup to demonstrate that we can learn the kernel parameters even if the data is not aligned with the candidate sensor placement locations, or is from a different environment altogether.

We now demonstrate our sensor placement approach for sensors with non-point FoV and integrated observations. We do this by considering the sensor placement for the sparse view CT scanning problem (Longi et al. [2020]). We used the whole observation space as the region of interest. We computed the solution sensor placements for 5 to 75 sensors (in increments of 10) using our approaches and the mutual information-based approach presented in Longi et al. [2020] as a baseline. We present the RMSE scores of the CT scan dataset reconstructions obtained using the solution sensor placement locations, and the sensor placement algorithm runtimes in Figure 4a and Figure 4b, respectively. Further technical details of the experiment are presented in the appendix.

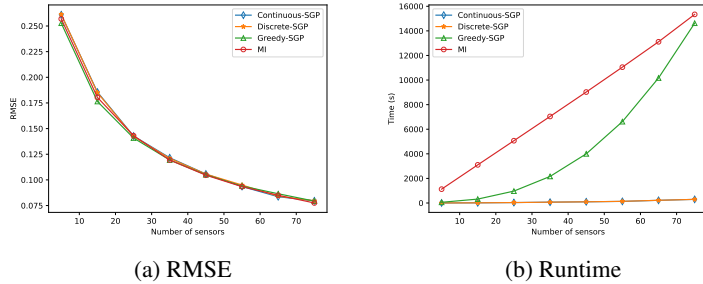


Figure 4: RMSE and runtime results for the CT scan dataset.

Our results show that our approaches are significantly faster (up to 53 times) while maintaining the reconstruction quality obtained using the computationally intensive MI-based approach. In the Greedy-SGP case, the method is still faster than the MI approach despite using a greedy optimization method. Also, the Continuous-SGP and Discrete-SGP approaches take a fraction of the computation time of the baseline MI approach and scale linearly with increasing sensing locations.

7 Conclusion

We addressed the sensor placement problem for monitoring spatially (or spatiotemporally) correlated data. We formulated the problem as a regression problem using SGPs and showed that training SGPs on unlabeled data gives us ideal sensor placements in continuous spaces. Furthermore, we presented an approach that uses the assignment problem to map the continuous domain solutions to discrete domains efficiently, giving us superior discrete solutions compared to the greedy approach. In addition, we generalized our approach to handle sensors with non-point FoV and integrated observations by leveraging the inherent properties of GPs and SGPs. We also compared and analysed our approach against the MI-based approach (Krause et al. [2008]). Our experiments on three real-world datasets demonstrated that our approaches result in reconstructions on par or better than the existing MI-based approaches while substantially reducing the computation time.

A key challenge for future work is to provide an approximation guarantee. We found that the SVGP’s lower bound is not submodular, and therefore cannot leverage the approximation guarantee of submodular functions. In addition, GP-based approaches rely on having accurate kernel function parameters for sensor placement. We aim to develop online approaches to address this in our future work. Our future work will also address related problems that require fast and efficient sensor placement such as sensor placement in linearly-constrained environments (Jidling et al. [2017]) and informative path planning (Ma et al. [2017]).

References

- Muhammad Asif Arain, Erik Schaffernicht, Victor Hernandez Bennetts, and Achim J. Lilienthal. The right direction to smell: Efficient sensor planning strategies for robot assisted gas tomography. In *2016 IEEE International Conference on Robotics and Automation (ICRA)*, pages 4275–4281, 2016.
- Matthias Bauer, Mark van der Wilk, and Carl Edward Rasmussen. Understanding Probabilistic Sparse Gaussian Process Approximations. In *Advances in Neural Information Processing Systems*, page 1533–1541, Red Hook, NY, USA, 2016.
- Christopher Bishop. *Pattern Recognition and Machine Learning*. Springer, New York, 2006.
- Peter Bodik, Wei Hong, Carlos Guestrin, Sam Madden, Mark Paskin, and Romain Thibaux. Intel lab data. *Online dataset*, 2004. URL <http://db.csail.mit.edu/labdata/labdata.html>.
- Christopher Bretherton, Martin Widmann, Valentin Dymnikov, John Wallace, and Ileana Bladé. The effective number of spatial degrees of freedom of a time-varying field. *Journal of Climate*, 12(7): 1990–2009, 1999.
- Thang D. Bui, Josiah Yan, and Richard E. Turner. A Unifying Framework for Gaussian Process Pseudo-Point Approximations Using Power Expectation Propagation. *Journal of Machine Learning Research*, 18(104):1–72, 2017.
- Rainer Burkard, Mauro Dell’Amico, and Silvano Martello. *Assignment Problems: revised reprint*. SIAM, Philadelphia, USA, 2012.
- David Burt, Carl Edward Rasmussen, and Mark Van Der Wilk. Rates of Convergence for Sparse Variational Gaussian Process Regression. In Kamalika Chaudhuri and Ruslan Salakhutdinov, editors, *Proceedings of the 36th International Conference on Machine Learning*, volume 97, pages 862–871. PMLR, Jun 2019.
- Mark de Berg, Otfried Cheong, Marc van Kreveld, and Mark Overmars. *Computational Geometry: Algorithms and Applications*. Springer-Verlag, Berlin, third edition, 2008.
- Oliver Hamelijnck, William J. Wilkinson, Niki Andreas Loppi, Arno Solin, and Theo Damoulas. Spatio-Temporal Variational Gaussian Processes. In A. Beygelzimer, Y. Dauphin, P. Liang, and J. Wortman Vaughan, editors, *Advances in Neural Information Processing Systems*, 2021.
- Trong Nghia Hoang, Quang Minh Hoang, and Bryan Kian Hsiang Low. A Unifying Framework of Anytime Sparse Gaussian Process Regression Models with Stochastic Variational Inference for Big Data. In Francis Bach and David Blei, editors, *Proceedings of the 32nd International Conference on Machine Learning*, volume 37, pages 569–578, Lille, France, 2015. PMLR.
- T. Husain and W. F. Caselton. Hydrologic Network Design Methods and Shannon’s Information Theory. *IFAC Proceedings Volumes*, 13(3):259–267, 1980. IFAC Symposium on Water and Related Land Resource Systems, Cleveland, OH, USA, May 1980.
- Kalvik Jakkala and Srinivas Akella. Probabilistic Gas Leak Rate Estimation Using Submodular Function Maximization With Routing Constraints. *IEEE Robotics and Automation Letters*, 7(2): 5230–5237, 2022.
- Carl Jidling, Niklas Wahlström, Adrian Wills, and Thomas B Schön. Linearly constrained Gaussian processes. In I. Guyon, U. Von Luxburg, S. Bengio, H. Wallach, R. Fergus, S. Vishwanathan, and R. Garnett, editors, *Advances in Neural Information Processing Systems*, volume 30. Curran Associates, Inc., 2017.
- Ma Jun, Ge Cheng, Wang Yixin, An Xingle, Gao Jiantao, Yu Ziqi, Zhang Mingqing, Liu Xin, Deng Xueyuan, Cao Shucheng, Wei Hao, Mei Sen, Yang Xiaoyu, Nie Ziwei, Li Chen, Tian Lu, Zhu Yuntao, Zhu Qiongjie, Dong Guoqiang, and He Jian. COVID-19 CT Lung and Infection Segmentation Dataset, April 2020. URL <https://doi.org/10.5281/zenodo.3757476>.
- Andreas Krause, Ajit Singh, and Carlos Guestrin. Near-Optimal Sensor Placements in Gaussian Processes: Theory, Efficient Algorithms and Empirical Studies. *Journal of Machine Learning Research*, 9(8):235–284, 2008.

- Krista Longi, Chang Rajani, Tom Sillanpää, Joni Mäkinen, Timo Rauhala, Ari Salmi, Edward Haeggström, and Arto Klami. Sensor Placement for Spatial Gaussian Processes with Integral Observations. In Jonas Peters and David Sontag, editors, *Proceedings of the 36th Conference on Uncertainty in Artificial Intelligence (UAI)*, volume 124 of *Proceedings of Machine Learning Research*, pages 1009–1018. PMLR, 03–06 Aug 2020.
- Kai-Chieh Ma, Lantao Liu, and Gaurav S. Sukhatme. Informative Planning and Online Learning with Sparse Gaussian Processes. In *2017 IEEE International Conference on Robotics and Automation (ICRA)*, pages 4292–4298, 2017.
- Alexander G. de G. Matthews, James Hensman, Richard Turner, and Zoubin Ghahramani. On Sparse Variational Methods and the Kullback-Leibler Divergence between Stochastic Processes. In Arthur Gretton and Christian C. Robert, editors, *Proceedings of the 19th International Conference on Artificial Intelligence and Statistics*, volume 51, pages 231–239, Cadiz, Spain, May 2016. PMLR.
- Joaquin Quinonero-Candela, Carl Edward Rasmussen, and Christopher K. I. Williams. Approximation Methods for Gaussian Process Regression. In *Large-Scale Kernel Machines*, pages 203–223. MIT Press, 2007.
- Carl Edward Rasmussen and Christopher K. I. Williams. *Gaussian Processes for Machine Learning*. MIT Press, Cambridge, USA, 2005.
- M. C. Shewry and H. P. Wynn. Maximum entropy sampling. *Journal of Applied Statistics*, 14(2): 165–170, 1987.
- Edward Snelson and Zoubin Ghahramani. Sparse Gaussian Processes using Pseudo-inputs. In Y. Weiss, B. Schölkopf, and J. Platt, editors, *Advances in Neural Information Processing Systems*, volume 18. MIT Press, 2006.
- Varun Suryan and Pratap Tokekar. Learning a Spatial Field in Minimum Time With a Team of Robots. *IEEE Transactions on Robotics*, 36(5):1562–1576, 2020.
- Michalis Titsias. Variational Learning of Inducing Variables in Sparse Gaussian Processes. In David van Dyk and Max Welling, editors, *Proceedings of the Twelfth International Conference on Artificial Intelligence and Statistics*, pages 567–574, Florida, USA, 2009. PMLR.
- Joshua Whitman, Harshal Maske, Hassan A. Kingravi, and Girish Chowdhary. Evolving Gaussian Processes and Kernel Observers for Learning and Control in Spatiotemporally Varying Domains: With Applications in Agriculture, Weather Monitoring, and Fluid Dynamics. *IEEE Control Systems*, 41:30–69, 2021.
- William J. Wilkinson, Simo Särkkä, and Arno Solin. Bayes-Newton Methods for Approximate Bayesian Inference with PSD Guarantees. *CoRR*, abs/2111.01721, 2021.
- Shiyong Wu and James V. Zidek. An entropy-based analysis of data from selected NADP/NTN network sites for 1983–1986. *Atmospheric Environment. Part A. General Topics*, 26(11):2089–2103, 1992.
- Gengsheng Lawrence Zeng. *Image Reconstruction: Applications in Medical Sciences*. De Gruyter, 2017.
- Hai Zhu, Jen Jen Chung, Nicholas R.J. Lawrance, Roland Siegwart, and Javier Alonso-Mora. Online Informative Path Planning for Active Information Gathering of a 3D Surface. In *2021 IEEE International Conference on Robotics and Automation (ICRA)*, pages 1488–1494, 2021.

Supplementary Material for Efficient Sensor Placement from Regression with Sparse Gaussian Processes in Continuous and Discrete Spaces

Kalvik Jakkala and Srinivas Akella*

Contents

A Related Work	3
A.1 Gaussian Processes	3
A.2 Geometric Approaches	3
A.3 Gaussian Process-based Approaches	3
B Algorithms	5
B.1 Continuous Space Solutions	5
B.2 Greedy Discrete Space Solutions	6
B.3 Gradient-based Discrete Space Solutions	7
B.4 Linear and Non-linear transformations in SGPs	8
C Theory	10
C.1 SVGP Lower Bound Delta Term Expansion	10
C.2 Theoretical Ramifications	11
D Additional Experiments	13
D.1 Spatiotemporal Sensor Placement	13
D.2 Non-point FoV Sensor Placement	13
E Main Experiment Details and Results	14
E.1 Experiment setup	14
E.2 Dataset Environment Layouts	14
E.3 Runtime vs Number of Sensors (Intel dataset)	15
E.4 Runtime vs Number of Sensors (Precipitation dataset)	16
E.5 Mutual information vs Number of Sensors (Intel dataset)	17

*The authors are with the Computer Science Department, University of North Carolina at Charlotte, Charlotte, NC, USA. Email:{kjakkala, sake11a}@unc.edu. This work was funded in part by the UNC Charlotte Office of Research and Economic Development and by NSF under Award Number IIP-1919233.

E.6	Mutual information vs Number of Sensors (Precipitation dataset)	18
E.7	KL divergence vs Number of Sensors (Intel dataset)	19
E.8	KL divergence vs Number of Sensors (Precipitation dataset)	20
E.9	CT Scan dataset experiment details	21

A Related Work

A.1 Gaussian Processes

Building on prior GP approaches, [Murray-Smith and Pearlmutter \[2005\]](#) presented an approach that leverages linear transformations on Gaussian process priors to model ill-posed inverse problems and reduce the computational complexity of Gaussian processes.

[Lázaro-Gredilla and Figueiras-Vidal \[2009\]](#) developed Inter-Domain Gaussian processes (IDGPs) which could be used to form the support set of input features in domains different from the input features' original domain. The approach makes it possible to find sparser data representations, provided that one uses an appropriate transformation of the input features to parametrize the GP.

Recently, [Hamelijnck et al. \[2021\]](#) presented an SVGP approach that can model spatiotemporal data that is linear in the number of time steps. In addition, [Wilkinson et al. \[2021\]](#) presented an efficient stochastic gradient descent-based SGP. The method even accommodates non-Gaussian likelihood models and combines second-order Newtonian optimization techniques to improve model convergence.

A.2 Geometric Approaches

Early approaches to the sensor placement problem ([Bai et al. \[2006\]](#), [Ramsden \[2009\]](#)) used geometric models of the sensor's field of view to account for the region covered by each sensor and used computational geometry or integer programming methods to find solutions. Such approaches proved useful for problems such as the art gallery problem ([de Berg et al. \[2008\]](#)), which requires one to place cameras so that the entire environment is visible. However, these approaches do not consider the spatial correlations in the environment.

The coverage problem is also studied in robotics ([Cortes et al. \[2004\]](#), [Breitenmoser et al. \[2010\]](#), [Sadeghi et al. \[2022\]](#)). Similar to geometric approaches, authors focus on coverage by leveraging Voronoi decompositions ([de Berg et al. \[2008\]](#)). A few authors ([Schwager et al. \[2017\]](#), [Salam and Hsieh \[2019\]](#)) have even considered Gaussian kernel functions, but they did not leverage Gaussian processes.

A.3 Gaussian Process-based Approaches

Gaussian process (GP) based approaches addressed the limitations of geometric model-based sensor placement approaches by learning the spatial correlations in the environment. The learned GP is then used to quantify the information gained from each sensor placement while accounting for the correlations of the data field. However, these methods introduce severe computational scaling issues and require one to discretize the environment. Our method finds sensor locations in continuous spaces and overcomes the computational scaling issues.

Early GP-based approaches ([Shewry and Wynn \[1987\]](#), [Wu and Zidek \[1992\]](#)) placed sensors at the highest entropy locations. However, since GPs have high variance in regions of the environment far from the locations of the training samples, such approaches tended to place sensors at the sensing area's borders, resulting in poor coverage of the area of interest.

[Krause et al. \[2008\]](#) used mutual information (MI) computed with GPs to select sensor locations with the maximal information about all the unsensed locations in the environment. The approach avoided placing the sensors at the environment's boundaries and outperformed all earlier approaches in terms of solution accuracy and computational cost. It leveraged submodularity ([Nemhauser et al. \[1978\]](#)) and used efficient greedy algorithms to sequentially select sensor placements. The approach required one to discretize the environment to be able to use the greedy algorithm. The greedy approach paired with the optimization objective's submodularity facilitated the method's approximation factor of $(1 - 1/e)$, provided that the environment was discretized with significantly more than $2s$ points, where s is the number of sensors. In addition, for n discrete candidate sensor locations in the environment, the MI-based approach has a computational complexity of $\mathcal{O}(sn^4)$. But, the LAZY-GREEDY algorithm ([Minoux \[1978\]](#)) can reduce the cost to $\mathcal{O}(sn^3)$ while retaining the approximation factor.

Whitman et al. [2021] recently proposed an approach to model spatiotemporal data fields using a combination of sparse Gaussian processes and state space models. They then used the spatiotemporal model to sequentially place sensors in a discretized version of the environment. Although their spatiotemporal model of the environment resulted in superior sensor placements, the combinatorial search becomes prohibitively large and limits the size of the problems that can be solved using the method.

Longi et al. [2020] addressed sensor placement for sparse view CT-scanning using the mutual information-based approach by Krause et al. [2008]. They leveraged the closed-form nature of Gaussian processes under linear transformations to extend the MI approach to handle the data-integrating sensor model of CT scanners. However, the method still relies on discrete optimization, which makes the approach computationally expensive and ill-suited for real-time applications.

B Algorithms

This section presents detailed algorithms for each of our sensor placement approaches—Continuous-SGP, Greedy-SGP, and Discrete-SGP.

B.1 Continuous Space Solutions

Algorithm 1: Continuous-SGP approach for obtaining sensor placements in continuous environments. Here k_θ is the kernel function with parameters learnt from either historical data or expert knowledge, Φ is a random distribution defined over the domain of the environment \mathcal{V} , s is the number of required sensors, n is the number of random locations used to train the SGP, and γ is the SGP learning rate.

Input: $k_\theta, \mathcal{V}, \Phi, s, n, \gamma$
Output: Solution sensor placements $\mathcal{A} \subset \mathcal{V}$, where $|\mathcal{A}| = s$

```
1  $\mathbf{X} = \{\emptyset\}$ ;  
  // Initialize empty set to store SGP training set  
2 repeat  
  | // Draw  $n$  random unlabeled locations from the environment  
3  |  $\mathbf{x} \sim \Phi(\mathcal{V})$   
4  |  $\mathbf{X} \leftarrow \mathbf{X} \cup \{\mathbf{x}\}$   
5 until  $|\mathbf{X}| = n$ ;  
6  $\mathcal{D} = (\mathbf{X}, \mathbf{y} = \mathbf{0})$ ;  
  // Generate SGP training dataset with 0 labels  
7  $\mathbf{X}_m = \text{RandomSubset}(\mathbf{X}, s)$ ;  
  // Initialize  $s$  inducing points at random locations  
8  $\varphi = \text{SGP}(0, k_\theta; \mathcal{D}, \mathbf{X}_m)$ ;  
  // Initialize a SVGP  $\varphi$  with 0 mean, kernel function  $k_\theta$ , training  
  // set  $\mathcal{D}$ , and inducing points  $\mathbf{X}_m$   
9 repeat  
10 |  $\mathbf{X}_m \leftarrow \mathbf{X}_m + \gamma \nabla \mathcal{F}_\varphi(\mathbf{X}_m)$ ;  
   | // Optimize the inducing point locations  $\mathbf{X}_m$  by maximizing the  
   | // SVGP's ELBO  $\mathcal{F}_\varphi$  using gradient ascent with a learning rate of  
   | //  $\gamma$   
11 until convergence;  
12 return  $\mathbf{X}_m$ 
```

B.2 Greedy Discrete Space Solutions

Algorithm 2: Greedy-SGP approach for obtaining sensor placements in discrete environments (i.e., sensor placements limited to a given set of candidate sensor locations) using a greedy selection approach. Here k_θ is the kernel function with parameters learnt from either historical data or expert knowledge, \mathcal{S} is the set of candidate sensor placement locations, Φ is a random distribution defined over the domain of the environment \mathcal{V} , and s is the number of required sensors, n is the number of random locations used to train the SGP.

Input: $k_\theta, \mathcal{V}, \mathcal{S}, \Phi, s, n$

Output: Solution sensor placements $\mathcal{A} \subset \mathcal{S}$, where $|\mathcal{A}| = s$

```

1  $\mathbf{X} = \{\emptyset\}$ ;
  // Initialize empty set to store SGP training set
2 repeat
  // Draw  $n$  random unlabeled locations from the environment
3    $\mathbf{x} \sim \Phi(\mathcal{V})$ 
4    $\mathbf{X} \leftarrow \mathbf{X} \cup \{\mathbf{x}\}$ 
5 until  $|\mathbf{X}| = n$ ;
6  $\mathcal{D} = (\mathbf{X}, \mathbf{y} = \mathbf{0})$ ;
  // Generate SGP training dataset with 0 labels
7  $\varphi = \text{SGP}(0, k_\theta; \mathcal{D})$ ;
  // Initialize a SVGP  $\varphi$  with 0 mean, kernel function  $k_\theta$ , and
  // training set  $\mathcal{D}$ 
8 repeat
  /* Sequentially select each of the solution inducing point locations
  using the greedy approach. */
9    $\mathbf{X}_m \leftarrow \mathbf{X}_m \cup \{\arg \max_{\mathbf{x} \in \mathcal{S} \setminus \mathbf{X}_m} \mathcal{F}_\varphi(\mathbf{X}_m \cup \{\mathbf{x}\}) - \mathcal{F}_\varphi(\mathbf{X}_m)\}$ 
10 until  $|\mathbf{X}_m| = s$ ;
11 return  $\mathbf{X}_m$ 

```

B.3 Gradient-based Discrete Space Solutions

Algorithm 3: Discrete-SGP approach for obtaining sensor placements in discrete environments (i.e., sensor placements limited to a given set of candidate sensor locations) using gradient descent. Here k_θ is the kernel function with parameters learnt from either historical data or expert knowledge, \mathcal{S} is the set of candidate sensor placement locations, Φ is a random distribution defined over the domain of the environment \mathcal{V} , s is the number of required sensors, n is the number of random locations used to train the SGP, and γ is the SGP learning rate.

Input: $k_\theta, \mathcal{V}, \mathcal{S}, \Phi, s, n, \gamma$

Output: Solution sensor placements $\mathcal{A} \subset \mathcal{S}$, where $|\mathcal{A}| = s$

```
1  $\mathbf{X}_m = \text{Continuous-SGP}(k_\theta, \mathcal{V}, \Phi, s, n, \gamma)$  ;  
   // Get the  $s$  continuous space sensor placements using  
   // our gradient based approach  
   // Continuous-SGP (Algorithm 1)  
2  $\mathbf{C} = \mathbf{0}^{|\mathbf{X}_m| \times |\mathcal{S}|}$  ;  
   // Initialize zero matrix to store pairwise distances  
3 for  $i \leftarrow 0$  to  $|\mathbf{X}_m|$  do  
4   for  $j \leftarrow 0$  to  $|\mathcal{S}|$  do  
5      $\mathbf{C}[i][j] \leftarrow \|\mathbf{X}_m[i] - \mathcal{S}[j]\|_2$  ;  
     // Compute the pairwise  $L_2$  distances  
6  $A = \mathcal{H}(\mathbf{C})$  ;  
   // Solve the assignment problem  $\mathcal{H}$  (Burkard et al. [2012]) to assign the  
   //  $s$  continuous space inducing points  $\mathbf{X}_m$  to  $s$  locations in the  
   // candidate sensor placement locations set  $\mathcal{S}$   
7  $\mathbf{X}_m^* = \mathcal{S}[A]$  ;  
   // Use the solution assignments  $A$  to index the candidate sensor  
   // placement locations set  $\mathcal{S}$  and get the solution discrete sensor  
   // placements  
8 return  $\mathbf{X}_m^*$ 
```

B.4 Linear and Non-linear transformations in SGPs

Algorithm 4: Expansion and aggregation transformation based approach for obtaining non-point FoV sensor placements. Here k_θ is the kernel function with parameters learnt from either historical data or expert knowledge, Φ is a random distribution defined over the domain of the environment \mathcal{V} , s is the number of required sensors, n is the number of random locations used to train the SGP, and γ is the SGP learning rate. T_{exp} and T_{agg} are the expansion and aggregation transformations, respectively.

Input: $k_\theta, \mathcal{V}, \Phi, s, n, \gamma, T_{\text{exp}}, T_{\text{agg}}$
Output: Solution sensor placements $\mathcal{A} \subset \mathcal{V}$, where $|\mathcal{A}| = s$

```

1  $\mathbf{X} = \{\emptyset\}$ ;
  // Initialize empty set to store SGP training set
2 repeat
  // Draw  $n$  random unlabeled locations from the environment
3    $\mathbf{x} \sim \Phi(\mathcal{V})$ 
4    $\mathbf{X} \leftarrow \mathbf{X} \cup \{\mathbf{x}\}$ 
5 until  $|\mathbf{X}| = n$ ;
6  $\mathcal{D} = (\mathbf{X}, \mathbf{y} = \mathbf{0})$ ;
  // Generate SGP training dataset with 0 labels
7  $\mathbf{X}_m = \text{RandomSubset}(\mathbf{X}, s)$ ;
  // Initialize  $s$  inducing points at random locations
8  $\mathbf{X}_m \leftarrow \text{RandomTheta}(\mathbf{X}_m, s)$ ;
  // Add random sampled angles as the rotation parameter of each
  // inducing point
9  $\varphi = \text{SGP}(0, k_\theta; \mathcal{D}, \mathbf{X}_m)$ ;
  // Initialize a SVGP  $\varphi$  with 0 mean, kernel function  $k_\theta$ , training
  // set  $\mathcal{D}$ , and inducing points  $\mathbf{X}_m$ 
10 repeat
11    $\mathbf{X}_{mp} = T_{\text{exp}}(\mathbf{X}_m)$ ;
  // Use the expansion transformation  $T_{\text{exp}}$  to map the  $m$  inducing
  // points  $\mathbf{X}_m$  in the point parametrization to  $mp$  points with FoV
  // parametrization
12    $\mathbf{Q}_{nn} = (\mathbf{K}_{n \times mp} T_{\text{agg}})(T_{\text{agg}}^\top \mathbf{K}_{mp \times mp}^{-1} T_{\text{agg}})(T_{\text{agg}}^\top \mathbf{K}_{mp \times n})$ ;
  // Use the aggregation transformation  $T_{\text{agg}}$ 
  // to reduce the covariances
13    $\mathbf{X}_m \leftarrow \mathbf{X}_m + \gamma \nabla \mathcal{F}_\varphi(\mathbf{Q}_{nn})$ ;
  // Optimize the point parametrized inducing points  $\mathbf{X}_m$  by
  // maximizing the SVGP's ELBO  $\mathcal{F}_\varphi$  using gradient descent (ascent)
  // with a learning rate of  $\gamma$ . We compute the ELBO using the  $\mathbf{Q}_{nn}$ 
  // computed above
14 until convergence;
15 return  $\mathbf{X}_m$ 

```

Consider a 2-dimensional sensor placement environment. Each of the point parametrized inducing points $\mathbf{X}_m \in \mathbb{R}^{m \times 2}$, are mapped to p points ($\mathbf{X}_{mp} \in \mathbb{R}^{mp \times 2}$) using the expansion transformation T_{exp} . This approach scales to any higher dimensional sensor placement environment and can even include additional variables such as the orientation and scale of the sensor/FoV, such as when considering the FoV of a camera on an aerial drone.

The following is an example of the expansion transformation operation written as a function in Python with TensorFlow. The function considers sensor with a FoV shaped as a line with a fixed length.

Algorithm 5: Expansion transformation function (written in Python with TensorFlow (Abadi et al. [2016])) used to map the 2D position (x, y) and orientation (θ) to a set of points along a line segment with the origin at the 2D point in the direction of the orientation θ . Here, \mathbf{X}_m are the inducing points with the position and orientation parameterization, l is the length of the line along which the mapped points are sampled, and p is the number of points that are sampled along the line.

```

1 Input:  $\mathbf{X}_m, l, p$ 
2  $x, y, \theta = \text{tf.split}(\mathbf{X}_m, \text{num\_or\_size\_splits} = 3, \text{axis} = 1)$ 
3  $x = \text{tf.squeeze}(x)$ 
4  $y = \text{tf.squeeze}(y)$ 
5  $\theta = \text{tf.squeeze}(\theta)$ 
6  $\mathbf{X}_m = \text{tf.linspace}([x, y], [x + l \times \text{tf.cos}(\theta), y + l \times \text{tf.sin}(\theta)], p, \text{axis} = 1)$ 
7  $\mathbf{X}_m = \text{tf.transpose}(\mathbf{X}_m, [2, 1, 0])$ 
8  $\mathbf{X}_m = \text{tf.reshape}(\mathbf{X}_m, [-1, 2])$ 
9 return  $\mathbf{X}_m$ 

```

The aggregation transformation matrix $T_{\text{agg}} \in \mathbb{R}^{mp \times m}$ is populated as follows for $m = 3$ and $p = 2$ for mean aggregation:

$$T_{\text{agg}}^{\top} = \begin{bmatrix} 0.5 & 0.5 & 0 & 0 & 0 & 0 \\ 0 & 0 & 0.5 & 0.5 & 0 & 0 \\ 0 & 0 & 0 & 0 & 0.5 & 0.5 \end{bmatrix}.$$

However, one can even use the 1-dimensional average pooling operation to efficiently apply the aggregation transformation without having to store large aggregation matrices.

C Theory

C.1 SVGP Lower Bound Delta Term Expansion

This section shows the derivation of the SVGP lower bound’s delta term used to contrast with the MI approach’s delta term (Krause et al. [2008]).

Entropy Properties:

1. Joint entropy can be decomposed into the sum of conditional entropy and marginal entropy (Bishop [2006]):

$$\begin{aligned} H(X, Y) &= H(X|Y) + H(Y) \\ &= H(Y|X) + H(X). \end{aligned}$$

2. The reverse KL divergence is the cross entropy minus entropy (Murphy [2022]):

$$\text{KL}(q||p) = H_p(q) - H(q).$$

Sparse Variational Gaussian Process (SVGP, Titsias [2009]): The lower bound of the SVGP is given by:

$$\mathcal{F} = \frac{n}{2} \log(2\pi) + \frac{1}{2} \log |\mathbf{Q}_{nn} + \sigma_{\text{noise}}^2 I| + \frac{1}{2} \mathbf{y}^\top (\mathbf{Q}_{nn} + \sigma_{\text{noise}}^2 I)^{-1} \mathbf{y} - \frac{1}{2\sigma_{\text{noise}}^2} \text{Tr}(\mathbf{K}_{nn} - \mathbf{Q}_{nn}), \quad (1)$$

where \mathbf{K}_{nn} is the covariance matrix computed using the SGP’s kernel function on the n training samples \mathbf{X} , $\mathbf{Q}_{nn} = \mathbf{K}_{nm} \mathbf{K}_{mm}^{-1} \mathbf{K}_{mn}$, the subscript m corresponds to the inducing points set, σ_{noise} is the noise variance, and \mathbf{y} is the vector containing the training set labels.

SVGP Lower Bound Delta Term Expansion: Assume that the inducing points are a subset of the training set indexed by $m \subset \{1, \dots, n\}$. Let $(\mathbf{X}_m, \mathbf{f}_m)$ be the set of inducing points locations and their corresponding latent variables. Similarly, let (\mathbf{X}, \mathbf{f}) be the training set locations and latent variables. Here n is the index set corresponding to the training dataset, and m is the index set corresponding to the inducing points. Note that we use the same notation as Titsias [2009], who also used n and m to denote the cardinality of these sets. We know that the SVGP lower bound (ELBO) can be written as follows (Bishop [2006]) for inducing points \mathbf{X}_m :

$$\begin{aligned} \mathcal{F}(\mathbf{X}_m) &= -\text{KL}(q_m(\mathbf{f})||p(\mathbf{f}|\mathbf{y})) + \log p(\mathbf{y}) \\ &= -H_{p(\mathbf{f}|\mathbf{y})}(q_m(\mathbf{f})) + H(q_m(\mathbf{f})) + \log p(\mathbf{y}). \end{aligned} \quad (2)$$

Here q_m is the variational distribution of the SGP with the m inducing points. We index the n training set points excluding the m inducing set points as the set difference $n - m$. We can use the above to formulate the increments in the SVGP lower bound upon adding a new inducing point \mathbf{x}_i such that $i \in n - m$ as follows:

$$\begin{aligned} \Delta \mathcal{F}(\mathbf{X}_m, \{\mathbf{x}_i\}) &= \mathcal{F}(\mathbf{X}_m \cup \{\mathbf{x}_i\}) - \mathcal{F}(\mathbf{X}_m) \\ &= -\text{KL}(q_{m+1}(\mathbf{f})||p(\mathbf{f}|\mathbf{y})) + \text{KL}(q_m(\mathbf{f})||p(\mathbf{f}|\mathbf{y})) \\ &= -H_{p(\mathbf{f}|\mathbf{y})}(q_{m+1}(\mathbf{f})) + H(q_{m+1}(\mathbf{f})) + H_{p(\mathbf{f}|\mathbf{y})}(q_m(\mathbf{f})) - H(q_m(\mathbf{f})) \\ &= \underbrace{(H(q_{m+1}(\mathbf{f})) - H(q_m(\mathbf{f})))}_{\Delta h_1} - \underbrace{(H_{p(\mathbf{f}|\mathbf{y})}(q_{m+1}(\mathbf{f})) - H_{p(\mathbf{f}|\mathbf{y})}(q_m(\mathbf{f})))}_{\Delta h_2}. \end{aligned} \quad (3)$$

The last equation above is similar to the KL divergence, except that each entropy term here Δh_j is the difference of two entropies. We can use the following expansion of the variational distribution q_m to simplify the above:

$$\begin{aligned}
q_m(\mathbf{f}) &= p(\mathbf{f}_{n-(m+1)}, f_i | \mathbf{f}_m) \phi(\mathbf{f}_m) \\
&= p(\mathbf{f}_{n-(m+1)} | f_i, \mathbf{f}_m) p(f_i | \mathbf{f}_m) \phi(\mathbf{f}_m).
\end{aligned} \tag{4}$$

Here we factorized the variational distribution over \mathbf{f} as the product of the variational distribution ϕ over the latents \mathbf{f}_m parametrized with the m inducing points \mathbf{X}_m and the conditional distribution p over the remaining data points $n - m$ computed using conditioning; f_i corresponds to the additional data sample added to the m inducing points. Similar to the above we can expand $q_{m+1}(\mathbf{f})$ as follows:

$$\begin{aligned}
q_{m+1}(\mathbf{f}) &= p(\mathbf{f}_{n-(m+1)} | \mathbf{f}_{m+1}) \phi(\mathbf{f}_{m+1}) \\
&= p(\mathbf{f}_{n-(m+1)} | \mathbf{f}_m, f_i) \phi(f_i | \mathbf{f}_m) \phi(\mathbf{f}_m).
\end{aligned} \tag{5}$$

Instead of using the conditional $p(f_i | \mathbf{f}_m)$ as we did for $q_m(\mathbf{f})$, here the distribution over f_i is from the variational distribution $\phi(f_i | \mathbf{f}_m)$. Since all the inducing points are explicitly given in the variational distribution, the joint variational distribution over the inducing points can be decomposed as the product of marginals. We can now plug the decomposed variational distribution back into Equation 3 to get the following using the chain rule of entropy:

$$\begin{aligned}
\Delta h_1 &= H(q_{m+1}(\mathbf{f})) - H(q_m(\mathbf{f})) \\
&= H(p(\mathbf{f}_{n-(m+1)} | f_i, \mathbf{f}_m) \phi(f_i | \mathbf{f}_m) \phi(\mathbf{f}_m)) - H(p(\mathbf{f}_{n-(m+1)} | f_i, \mathbf{f}_m) p(f_i | \mathbf{f}_m) \phi(\mathbf{f}_m)) \\
&= \cancel{H(p(\mathbf{f}_{n-(m+1)} | f_i, \mathbf{f}_m))} + H(\phi(f_i | \mathbf{f}_m)) + \cancel{H(\phi(\mathbf{f}_m))} - \cancel{H(p(\mathbf{f}_{n-(m+1)} | f_i, \mathbf{f}_m))} - H(p(f_i | \mathbf{f}_m)) - \cancel{H(\phi(\mathbf{f}_m))} \\
&= H(\phi(f_i | \mathbf{f}_m)) - H(p(f_i | \mathbf{f}_m)).
\end{aligned} \tag{6}$$

Similar to the above, we can get $\Delta h_2 = H_{p(f_i | \mathbf{y})}(\phi(f_i | \mathbf{f}_m)) - H_{p(f_i | \mathbf{y})}(p(f_i | \mathbf{f}_m))$. This gives us the following:

$$\begin{aligned}
\Delta \mathcal{F}(\mathbf{X}_m, \{\mathbf{x}_i\}) &= H(\phi(f_i | \mathbf{f}_m)) - H(p(f_i | \mathbf{f}_m)) - H_{p(f_i | \mathbf{y})}(\phi(f_i | \mathbf{f}_m)) + H_{p(f_i | \mathbf{y})}(p(f_i | \mathbf{f}_m)) \\
&= (H(\phi(f_i | \mathbf{f}_m)) - H_{p(f_i | \mathbf{y})}(\phi(f_i | \mathbf{f}_m))) - (H(p(f_i | \mathbf{f}_m)) - H_{p(f_i | \mathbf{y})}(p(f_i | \mathbf{f}_m))) \\
&= \text{KL}(\phi(f_i | \mathbf{f}_m) || p(f_i | \mathbf{y})) - \text{KL}(p(f_i | \mathbf{f}_m) || p(f_i | \mathbf{y})).
\end{aligned} \tag{7}$$

SVGP Lower Bound's Submodularity: We also checked to see if the SVGP bound is submodular, but we could not prove it mathematically. Consider $\mathbf{X}_m \subseteq \mathbf{X}_l \subset \mathbf{X}$ and $\mathbf{x}_i \in \mathbf{X} \setminus \mathbf{X}_l$:

$$\begin{aligned}
&\Delta \mathcal{F}(\mathbf{X}_m, \{\mathbf{x}_i\}) - \Delta \mathcal{F}(\mathbf{X}_l, \{\mathbf{x}_i\}) \geq 0 \\
&\text{KL}(\phi(f_i | \mathbf{f}_m) || p(f_i | \mathbf{y})) - \text{KL}(p(f_i | \mathbf{f}_m) || p(f_i | \mathbf{y})) - \text{KL}(\phi(f_i | \mathbf{f}_l) || p(f_i | \mathbf{y})) + \text{KL}(p(f_i | \mathbf{f}_l) || p(f_i | \mathbf{y})) \geq 0
\end{aligned} \tag{8}$$

One needs to show that the last equation above is true for the SVGP to be submodular. We empirically found that it is indeed not a submodular function.

C.2 Theoretical Ramifications

We can gain insights into the performance of our SGP based sensor placement approach from the SGP literature:

1. We can use the bound on the KL divergence in SVGPs (Burt et al. [2019]) to evaluate the quality of the learned inducing points set's approximation of the full GP, i.e., the quality of the solution sensor placements' approximation of the data field in the environment. This applies to all our sensor placement approaches.
2. From Burt et al. [2019], under certain conditions, we know that $\mathcal{O}(\log^d n)$ inducing points are sufficient to make the KL divergence between the variational distribution of the SGP and the full GP arbitrarily small, where n is the number of points in the training set and d is

the dimensionality of the training data. Therefore our approach even suggests a minimum cardinality constraint required to get accurate results.

D Additional Experiments

D.1 Spatiotemporal Sensor Placement

We demonstrate our approach’s scalability to large spatiotemporal data fields by finding placements for 500 ozone concentration sensors across the planet. Note that the environment is the surface of a sphere in this example. We used a spatiotemporal-sparse variational Gaussian process (ST-SVGP, Hamelijnc et al. [2021]) as it allows us to efficiently model spatiotemporal correlations in the data with time complexity linear in the number of time steps in the training set. We used Matern 3/2 kernels (Rasmussen and Williams [2005]) to model the spatial and temporal correlations. All the model parameters were optimized with a learning rate of 0.01, and the parameters were optimized using the Adam optimizer (Kingma and Ba [2015]). The ST-SVGP was trained on the first six months of the monthly ozone data from 2018 (Service [2018]). We used a subset of 1040 uniformly distributed locations in the dataset as the training set and 100 inducing points to learn the kernel parameters. The learned kernel function was then used in our sensor placement approach—Continuous-SGP (Algorithm 1)—to obtain the 500 solution placements shown below.

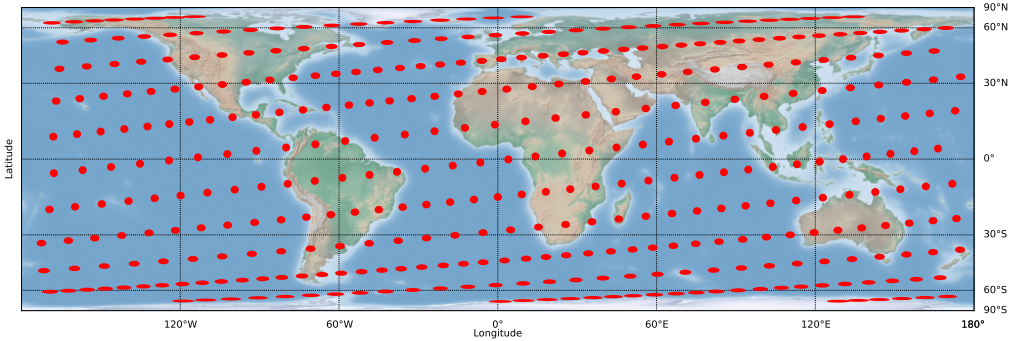


Figure 1: 500 sensor placements generated using the Continuous-SGP approach with an ST-SVGP (Hamelijnc et al. [2021]). The red points are the sensor placements projected onto the 2D map using cylindrical equal-area projection.

As expected, the solution placements are relatively uniformly distributed over the planet. This is because we used a stationary kernel function. However, in a real-world scenario, using a non-stationary kernel would give us even more informative sensing locations that can further leverage the non-stationary nature of the environment.

D.2 Non-point FoV Sensor Placement

We now present our solution sensor placements for non-point FoV sensors in an environment with multiple obstacles (Figure 2). We used a rectangle with 36 points (9×4 points) for the FoV of the sensors. The sensor placements were obtained by augmenting an SGP with the expansion and aggregation transformations. The transformations allowed us to efficiently optimize the SGP while also accommodating the sensor’s non-point FoV. We trained the SGP using gradient descent on randomly sampled points in the environment where there were no obstacles and set all labels to zero. As we can see, the solution placements are well-spaced to ensure that the same information is not repeatedly collected. Also, our solution placements almost perfectly avoid the obstacles.

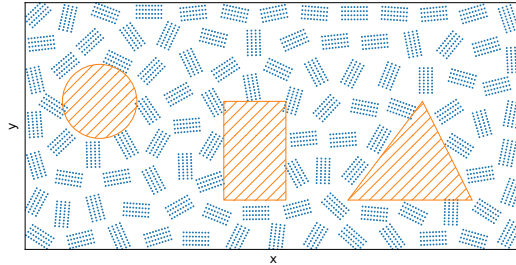


Figure 2: 100 sensor placements generated using an SGP augmented with the expansion transformation and aggregation transformation for sensors with a rectangular FoV. The hatched orange polygons represent obstacles in the environment. Each rectangular group of blue points represents the sensor’s FoV.

E Main Experiment Details and Results

E.1 Experiment setup

We used an RBF kernel (Rasmussen and Williams [2005]) in all our remaining experiments, and trained all GPs with a learning rate of $1e - 2$ for a maximum of 3000 iterations using the Adam optimizer (Kingma and Ba [2015]). We used the GPflow Python library (van der Wilk et al. [2020]) for all our GP implementations, and the apricot Python library (Schreiber et al. [2020]) for the greedy selection algorithm.

All our experiments were executed on a Dell workstation with an Intel(R) Xeon(R) W-2265 CPU, and 128 GB RAM. We ran our experiments in Python 3.8.10 running in Ubuntu 20.04.04 OS running in WSL 2 on Windows 11 OS.

E.2 Dataset Environment Layouts

The following are the environment layouts of the Intel and the precipitation datasets.

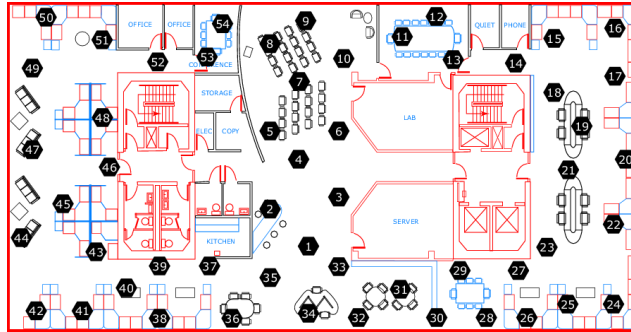


Figure 3: Intel dataset

Figure 4: Intel dataset layout. The black hexagons are the training set sensor locations.

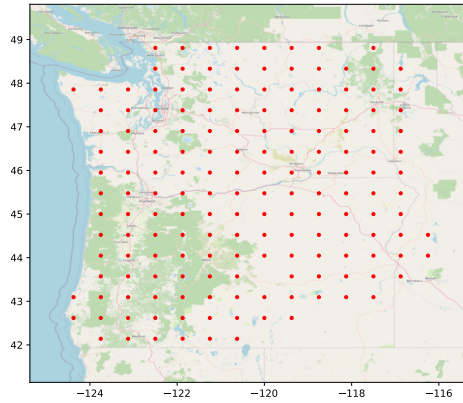


Figure 5: Precipitation dataset

Figure 6: Precipitation dataset layout. The red dots are the training set sensor locations.

E.3 Runtime vs Number of Sensors (Intel dataset)

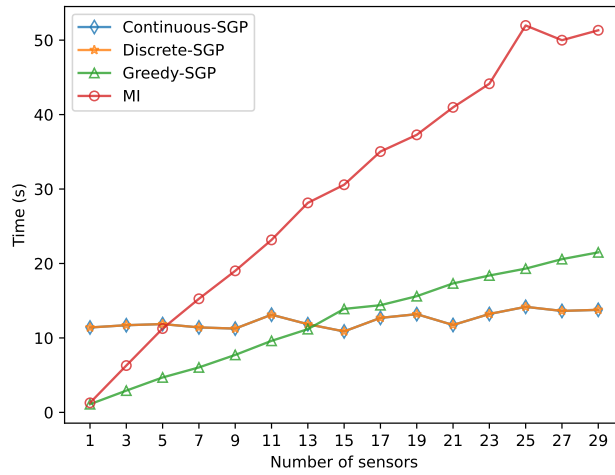


Figure 7: Runtime vs number of sensors for the Intel dataset (lower is better).

# Sensors	MI	Greedy-SGP	Discrete-SGP	Continuous-SGP
1	1.2812	1.0986	11.4042	11.4038
3	6.2916	2.9233	11.7086	11.7078
5	11.2585	4.6921	11.8633	11.8630
7	15.2582	6.0390	11.4133	11.4128
9	19.0114	7.7185	11.2550	11.2544
11	23.1663	9.6091	13.1198	13.1191
13	28.1402	11.1787	11.8443	11.8435
15	30.5757	13.8983	10.8750	10.8741
17	35.0339	14.3969	12.6928	12.6918
19	37.2780	15.6067	13.1926	13.1913
21	40.9678	17.3218	11.7385	11.7372
23	44.1415	18.3834	13.2163	13.2151
25	51.9692	19.3090	14.1771	14.1752
27	49.9905	20.5831	13.6288	13.6271
29	51.3212	21.4923	13.7737	13.7719

Table 1: Runtime for each of the approaches on the Intel dataset.

E.4 Runtime vs Number of Sensors (Precipitation dataset)

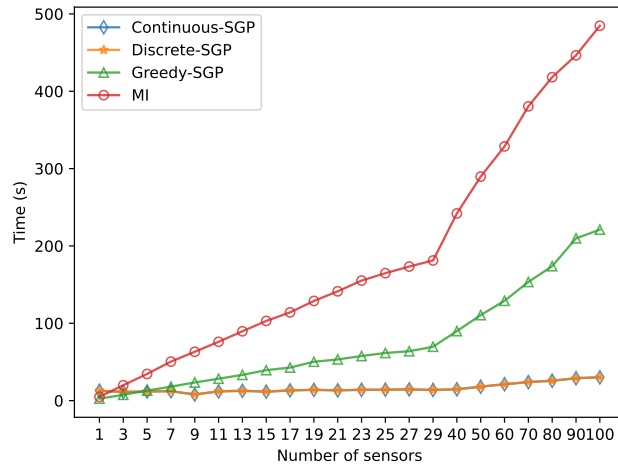


Figure 8: Runtime vs number of sensors for the precipitation dataset (lower is better).

# Sensors	MI	Greedy-SGP	Discrete-SGP	Continuous-SGP
1	4.7658	2.5163	12.7610	12.7593
3	19.9100	7.5177	11.2340	11.2324
5	34.4514	12.8595	11.7916	11.7898
7	50.4176	18.0651	12.1861	12.1843
9	63.1244	23.4340	7.9223	7.9200
11	76.0493	28.2837	11.9068	11.9047
13	89.6212	33.2389	12.7420	12.7392
15	103.0159	39.3639	11.5692	11.5670
17	114.1175	42.7027	13.2455	13.2428
19	128.8327	50.2084	13.9101	13.9076
21	141.3201	53.2547	13.2897	13.2872
23	155.1815	57.6343	13.9392	13.9357
25	164.7759	61.5781	14.1408	14.1373
27	173.3031	63.8479	14.4902	14.4865
29	181.1978	69.6146	13.8011	13.7976
40	241.9910	89.8695	14.6402	14.6364
50	289.6427	110.5149	17.9720	17.9683
60	328.6580	129.0436	21.1707	21.1671
70	380.4585	153.3872	23.9837	23.9811
80	418.1881	173.8247	25.6478	25.6433
90	446.4252	209.7938	28.9949	28.9910
100	484.6607	221.0156	30.1256	30.1211

Table 2: Runtime for each of the approaches on the precipitation dataset.

E.5 Mutual information vs Number of Sensors (Intel dataset)

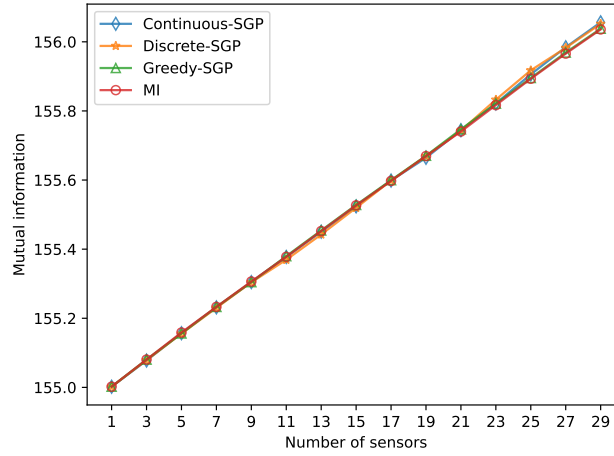


Figure 9: Mutual information vs number of sensors for the Intel dataset (higher is better).

# Sensors	MI	Greedy-SGP	Discrete-SGP	Continuous-SGP
1	154.6225	154.6225	154.6225	154.6223
3	154.7011	154.7011	154.6994	154.6983
5	154.7796	154.7769	154.7761	154.7776
7	154.8539	154.8538	154.8511	154.8525
9	154.9275	154.9256	154.9250	154.9257
11	154.9990	155.0010	154.9905	154.9987
13	155.0739	155.0756	155.0637	155.0720
15	155.1484	155.1495	155.1412	155.1455
17	155.2192	155.2214	155.2202	155.2203
19	155.2913	155.2922	155.2911	155.2862
21	155.3625	155.3689	155.3651	155.3664
23	155.4391	155.4434	155.4550	155.4438
25	155.5156	155.5179	155.5403	155.5286
27	155.5886	155.5916	155.6054	155.6072
29	155.6587	155.6608	155.6751	155.6795

Table 3: Mutual information of the solutions from each of the approaches on the Intel dataset.

E.6 Mutual information vs Number of Sensors (Precipitation dataset)

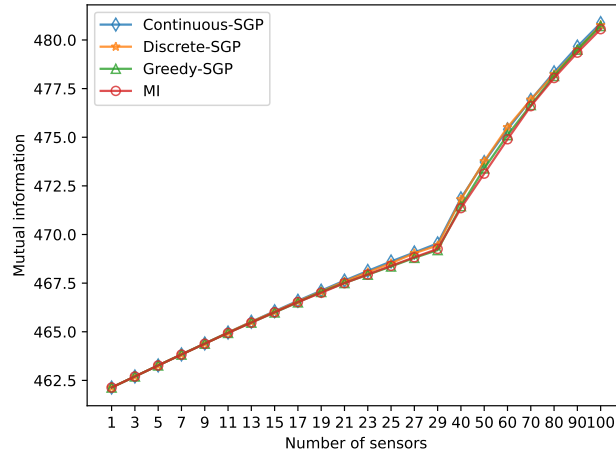


Figure 10: Mutual information vs number of sensors for the precipitation dataset (higher is better).

# Sensors	MI	Greedy-SGP	Discrete-SGP	Continuous-SGP
1	455.4251	455.4251	455.4251	455.4251
3	455.9993	455.9995	455.9995	455.9995
5	456.5727	456.5728	456.5739	456.5738
7	457.1394	457.1395	457.1469	457.1470
9	457.7021	457.7062	457.7133	457.7175
11	458.2658	458.2662	458.2827	458.2857
13	458.8013	458.8046	458.8429	458.8467
15	459.3429	459.3329	459.3687	459.3966
17	459.8742	459.8589	459.9044	459.9408
19	460.3585	460.4016	460.4207	460.4684
21	460.8637	460.8644	460.9501	460.9946
23	461.3131	461.3000	461.4284	461.4974
25	461.7651	461.7277	461.8991	461.9914
27	462.2095	462.1781	462.4201	462.4618
29	462.6455	462.5833	462.8264	462.9359
40	464.7733	464.8728	465.2359	465.2896
50	466.5727	466.8405	467.2224	467.1828
60	468.3645	468.5762	468.9911	468.8845
70	470.0918	470.1460	470.4297	470.4272
80	471.5600	471.6609	471.7547	471.8597
90	472.8822	473.0349	473.0315	473.2005
100	474.1054	474.2662	474.3137	474.4241

Table 4: Mutual information of the solutions from each of the approaches on the Intel dataset.

E.7 KL divergence vs Number of Sensors (Intel dataset)

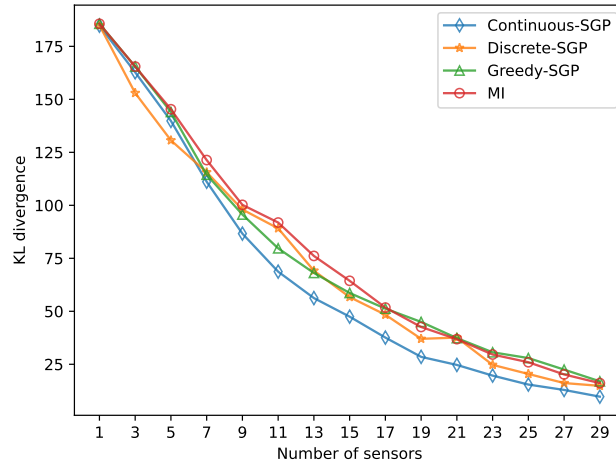


Figure 11: KL divergence between the SGP posterior and the true posterior (Burt et al. [2019]) vs number of sensors for the Intel dataset (lower is better).

# Sensors	MI	Greedy-SGP	Discrete-SGP	Continuous-SGP
1	186.1976	186.1976	185.4701	185.2974
3	166.0500	166.0500	153.5595	163.3587
5	145.9037	144.6126	131.2139	140.4108
7	121.9117	114.9829	116.1213	111.6662
9	100.7483	96.1549	98.5384	87.1225
11	92.3842	80.1849	89.6472	69.1503
13	76.5700	68.5222	69.6247	56.6379
15	64.7934	59.0565	57.1033	47.8304
17	52.1229	51.6477	48.7530	37.9037
19	42.9194	45.3418	37.3153	28.7573
21	37.1530	37.6714	37.9110	24.9260
23	29.8635	30.9328	24.9656	19.8604
25	26.1981	28.2032	20.6426	15.6039
27	20.4053	22.7156	16.3239	13.0423
29	16.2718	17.1314	14.9944	9.8440

Table 5: KL divergence between the SGP posterior and the true posterior (Burt et al. [2019]) of the solutions from each of the approaches on the Intel dataset.

E.8 KL divergence vs Number of Sensors (Precipitation dataset)

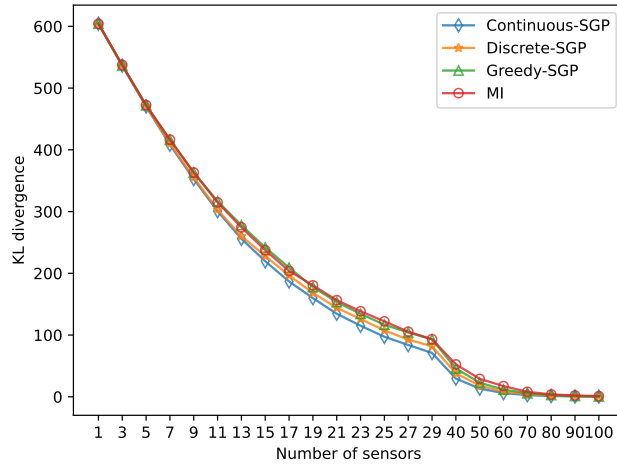


Figure 12: KL divergence between the SGP posterior and the true posterior (Burt et al. [2019]) vs number of sensors for the precipitation dataset (lower is better).

# Sensors	MI	Greedy-SGP	Discrete-SGP	Continuous-SGP
1	614.0881	614.0861	614.0934	614.0869
3	547.2524	546.3628	546.3105	546.1644
5	481.8775	481.5345	480.0815	479.8332
7	425.5199	425.4182	418.9677	417.2606
9	371.7843	371.8531	363.9170	361.2349
11	322.8112	324.7414	310.9479	308.6779
13	281.7597	285.3151	267.4849	263.2690
15	244.3067	248.7152	234.8825	226.2751
17	210.2184	215.4695	202.7956	192.9130
19	186.2311	183.5716	173.9968	165.3436
21	161.7331	158.7504	149.3590	139.4500
23	143.2397	139.1858	130.7278	119.5250
25	126.6179	121.2163	111.8190	101.1686
27	109.4382	108.3414	96.4733	87.4214
29	96.9322	96.7558	85.3363	74.1780
40	54.7927	48.0970	39.9946	31.1376
50	30.4784	24.1328	19.1166	14.1925
60	18.2545	12.4439	8.7220	6.4009
70	8.5995	6.1425	4.6070	2.9494
80	4.1045	3.1050	2.4642	1.3595
90	2.3026	1.3929	1.2021	0.5739
100	1.1720	0.5834	0.4978	0.2490

Table 6: KL divergence between the SGP posterior and the true posterior (Burt et al. [2019]) of the solutions from each of the approaches on the precipitation dataset.

E.9 CT Scan dataset experiment details

We used the COVID-19 CT scan dataset which contains lung scans from 10 patients, with each containing 301 slices (Jun et al. [2020]) to benchmark our sparse view CT scan sensor placements. We used a fan beam CT projection (Zeng [2017]) with 750 detectors with a width of 2. The source projection and the detector distance were set to 400. We used filter back projection (Zeng [2017]) from the ASTRA Toolbox (van Aarle et al. [2015]) to generate our reconstructions using the data from only the placement locations. The kernel parameters were learned from phantom CT images.

# Sensors	MI	Greedy-SGP	Discrete-SGP	Continuous-SGP
5	0.2569	0.2527	0.2613	0.2610
15	0.1804	0.1764	0.1851	0.1856
25	0.1431	0.1408	0.1424	0.1428
35	0.1194	0.1194	0.1210	0.1216
45	0.1046	0.1050	0.1056	0.1058
55	0.0934	0.0940	0.0950	0.0936
65	0.0850	0.0865	0.0841	0.0836
75	0.0775	0.0793	0.0796	0.0796

Table 7: RMSE vs number of sensors for the CT scan dataset (lower is better).

# Sensors	MI	Greedy-SGP	Discrete-SGP	Continuous-SGP
5	0.1021	0.0973	0.0932	0.0934
15	0.1475	0.1487	0.1438	0.1426
25	0.1960	0.1974	0.1993	0.1984
35	0.2323	0.2387	0.2317	0.2304
45	0.2700	0.2696	0.2685	0.2675
55	0.3029	0.2996	0.3014	0.3025
65	0.3308	0.3266	0.3351	0.3354
75	0.3592	0.3541	0.3569	0.3555

Table 8: SSIM vs number of sensors for the CT scan dataset (higher is better).

# Sensors	MI	Greedy-SGP	Discrete-SGP	Continuous-SGP
5	1125.9375	57.1025	4.0282	3.1066
15	3102.5137	318.3406	13.1679	13.0909
25	5066.4228	968.3583	35.8298	35.7661
35	7038.7364	2160.8199	67.9413	67.8967
45	9024.9766	3997.4588	96.5101	96.8211
55	11048.5689	6616.1409	135.8416	131.0395
65	13111.3387	10166.6850	219.5241	218.0974
75	15341.4043	14624.4529	295.5247	295.7489

Table 9: Runtime vs number of sensors for the CT scan dataset (lower is better).

References

- Martín Abadi, Paul Barham, Jianmin Chen, Zhifeng Chen, Andy Davis, Jeffrey Dean, Matthieu Devin, Sanjay Ghemawat, Geoffrey Irving, Michael Isard, et al. TensorFlow: A system for large-scale machine learning. In *12th USENIX Symposium on Operating Systems Design and Implementation (OSDI 16)*, pages 265–283, 2016.
- Xiaole Bai, Santosh Kumar, Dong Xuan, Ziqiu Yun, and Ten H. Lai. Deploying Wireless Sensors to Achieve Both Coverage and Connectivity. In *Proceedings of the 7th ACM International Symposium on Mobile Ad Hoc Networking and Computing*, page 131–142, New York, NY, USA, 2006.
- Christopher Bishop. *Pattern Recognition and Machine Learning*. Springer, New York, 2006.
- Andreas Breitenmoser, Mac Schwager, Jean-Claude Metzger, Roland Siegwart, and Daniela Rus. Voronoi coverage of non-convex environments with a group of networked robots. In *2010 IEEE International Conference on Robotics and Automation*, pages 4982–4989, 2010.
- Rainer Burkard, Mauro Dell’Amico, and Silvano Martello. *Assignment Problems: revised reprint*. SIAM, Philadelphia, USA, 2012.
- David Burt, Carl Edward Rasmussen, and Mark Van Der Wilk. Rates of Convergence for Sparse Variational Gaussian Process Regression. In Kamalika Chaudhuri and Ruslan Salakhutdinov, editors, *Proceedings of the 36th International Conference on Machine Learning*, volume 97, pages 862–871. PMLR, Jun 2019.
- Jorge Cortes, Sonia Martinez, Timur Karatas, and Francesco Bullo. Coverage control for mobile sensing networks. *IEEE Transactions on Robotics and Automation*, 20(2):243–255, 2004.
- Mark de Berg, Otfried Cheong, Marc van Kreveld, and Mark Overmars. *Computational Geometry: Algorithms and Applications*. Springer-Verlag, Berlin, third edition, 2008.
- Oliver Hamelijnck, William J. Wilkinson, Niki Andreas Loppi, Arno Solin, and Theo Damoulas. Spatio-Temporal Variational Gaussian Processes. In A. Beygelzimer, Y. Dauphin, P. Liang, and J. Wortman Vaughan, editors, *Advances in Neural Information Processing Systems*, 2021.
- Ma Jun, Ge Cheng, Wang Yixin, An Xingle, Gao Jiantao, Yu Ziqi, Zhang Mingqing, Liu Xin, Deng Xueyuan, Cao Shucheng, Wei Hao, Mei Sen, Yang Xiaoyu, Nie Ziwei, Li Chen, Tian Lu, Zhu Yuntao, Zhu Qiongjie, Dong Guoqiang, and He Jian. COVID-19 CT Lung and Infection Segmentation Dataset, April 2020. URL <https://doi.org/10.5281/zenodo.3757476>.
- Diederik P. Kingma and Jimmy Ba. Adam: A Method for Stochastic Optimization. In *International Conference on Learning Representations (Poster)*, 2015.
- Andreas Krause, Ajit Singh, and Carlos Guestrin. Near-Optimal Sensor Placements in Gaussian Processes: Theory, Efficient Algorithms and Empirical Studies. *Journal of Machine Learning Research*, 9(8):235–284, 2008.
- Miguel Lázaro-Gredilla and Aníbal R. Figueiras-Vidal. Inter-Domain Gaussian Processes for Sparse Inference Using Inducing Features. In *Advances in Neural Information Processing Systems*, page 1087–1095, Red Hook, NY, USA, 2009.
- Krista Longi, Chang Rajani, Tom Sillanpää, Joni Mäkinen, Timo Rauhala, Ari Salmi, Edward Haeggström, and Arto Klami. Sensor Placement for Spatial Gaussian Processes with Integral Observations. In Jonas Peters and David Sontag, editors, *Proceedings of the 36th Conference on Uncertainty in Artificial Intelligence (UAI)*, volume 124 of *Proceedings of Machine Learning Research*, pages 1009–1018. PMLR, 03–06 Aug 2020.
- Michel Minoux. Accelerated greedy algorithms for maximizing submodular set functions. In J. Stoer, editor, *Optimization Techniques*, pages 234–243, Berlin, Heidelberg, 1978. Springer.
- Kevin P. Murphy. *Probabilistic Machine Learning: An introduction*. MIT Press, Massachusetts, 2022.

- Roderick Murray-Smith and Barak A. Pearlmutter. Transformations of Gaussian Process Priors. In Joab Winkler, Mahesan Niranjan, and Neil Lawrence, editors, *Deterministic and Statistical Methods in Machine Learning*, pages 110–123, Berlin, Heidelberg, 2005. Springer.
- G. L. Nemhauser, L. A. Wolsey, and M. L. Fisher. An analysis of approximations for maximizing submodular set functions-I. *Mathematical Programming*, 14(1):265–294, Dec 1978.
- Daryn Ramsden. *Optimization approaches to sensor placement problems*. PhD thesis, Department of Mathematical Sciences, Rensselaer Polytechnic Institute, August 2009.
- Carl Edward Rasmussen and Christopher K. I. Williams. *Gaussian Processes for Machine Learning*. MIT Press, Cambridge, USA, 2005.
- Armin Sadeghi, Ahmad B. Asghar, and Stephen L. Smith. Distributed multi-robot coverage control of non-convex environments with guarantees. *IEEE Transactions on Control of Network Systems*, pages 1–12, 2022.
- Tahiya Salam and M. Ani Hsieh. Adaptive sampling and reduced-order modeling of dynamic processes by robot teams. *IEEE Robotics and Automation Letters*, 4(2):477–484, 2019.
- Jacob Schreiber, Jeffrey Bilmes, and William Stafford Noble. apricot: Submodular selection for data summarization in Python. *Journal of Machine Learning Research*, 21(161):1–6, 2020.
- Mac Schwager, Michael P. Vitus, Samantha Powers, Daniela Rus, and Claire J. Tomlin. Robust adaptive coverage control for robotic sensor networks. *IEEE Transactions on Control of Network Systems*, 4(3):462–476, 2017.
- Copernicus Climate Change Service. Ozone monthly gridded data from 1970 to present derived from satellite observations, 2018.
- M. C. Shewry and H. P. Wynn. Maximum entropy sampling. *Journal of Applied Statistics*, 14(2): 165–170, 1987.
- Michalis Titsias. Variational Learning of Inducing Variables in Sparse Gaussian Processes. In David van Dyk and Max Welling, editors, *Proceedings of the Twelfth International Conference on Artificial Intelligence and Statistics*, pages 567–574, Florida, USA, 2009. PMLR.
- Wim van Aarle, Willem Jan Palenstijn, Jan De Beenhouwer, Thomas Altantzis, Sara Bals, K. Joost Batenburg, and Jan Sijbers. The astra toolbox: A platform for advanced algorithm development in electron tomography. *Ultramicroscopy*, 157:35–47, 2015. ISSN 0304-3991.
- Mark van der Wilk, Vincent Dutordoir, ST John, Artem Artemev, Vincent Adam, and James Hensman. A Framework for Interdomain and Multioutput Gaussian Processes. *ArXiv*, 2020.
- Joshua Whitman, Harshal Maske, Hassan A. Kingravi, and Girish Chowdhary. Evolving Gaussian Processes and Kernel Observers for Learning and Control in Spatiotemporally Varying Domains: With Applications in Agriculture, Weather Monitoring, and Fluid Dynamics. *IEEE Control Systems*, 41:30–69, 2021.
- William J. Wilkinson, Simo Särkkä, and Arno Solin. Bayes-Newton Methods for Approximate Bayesian Inference with PSD Guarantees. *CoRR*, abs/2111.01721, 2021.
- Shiyong Wu and James V. Zidek. An entropy-based analysis of data from selected NADP/NTN network sites for 1983–1986. *Atmospheric Environment. Part A. General Topics*, 26(11):2089–2103, 1992.
- Gengsheng Lawrence Zeng. *Image Reconstruction: Applications in Medical Sciences*. De Gruyter, 2017.